




Evolution of the Stellar Mass Function and Infrared Luminosity Function of Galaxies since $z = 1.2$

Richard Beare¹, Michael J. I. Brown¹ , Kevin Pimbblet^{1,2}, and Edward N. Taylor³

¹ Monash Centre for Astrophysics, School of Physics and Astronomy, Monash University, Clayton, Victoria 3800, Australia; richard@beares.net

² E. A. Milne Centre for Astrophysics, University of Hull, Cottingham Road, Kingston-upon-Hull, HU6 7RX, UK

³ Centre for Astrophysics and Supercomputing, Swinburne University of Technology, Hawthorn, Victoria 3122, Australia

Received 2018 February 20; revised 2019 January 31; accepted 2019 February 2; published 2019 March 6

Abstract

We measured evolution of the K -band luminosity function and stellar mass function (SMF) for red and blue galaxies at $z < 1.2$ using a sample of 353 594 $I < 24$ galaxies in 8.26 square degrees of Boötes. We addressed several sources of systematic and random error in measurements of total galaxy light, photometric redshift, and absolute magnitude. We have found that the K -band luminosity density for both red and blue galaxies increased by a factor of 1.2 from $z \sim 1.1$ to $z \sim 0.3$, while the most luminous red (blue) galaxies decreased in luminosity by 0.19(0.33) mag or $\times 0.83(0.74)$. These results are consistent with $z < 0.2$ studies, while our large sample size and area result in smaller Poisson and cosmic variance uncertainties than most $z > 0.4$ luminosity and mass function measurements. Using an evolving relation for K -band mass-to-light ratios as a function of $(B-V)$ color, we found a slowly decreasing rate of growth in red galaxy stellar mass density of $\times 2.3$ from $z \sim 1.1$ to $z \sim 0.3$, indicating a slowly decreasing rate of migration from the blue cloud to the red sequence. Unlike some studies of the SMF, we find that massive red galaxies grow by a factor of $\times 1.7$ from $z \sim 1.1$ to $z \sim 0.3$, with the rate of growth due to mergers decreasing with time. These results are comparable with measurements of merger rates and clustering, and they are also consistent with the red galaxy stellar mass growth implied by comparing K -band luminosity evolution with the fading of passive stellar population models.

Key words: galaxies: abundances – galaxies: evolution – galaxies: luminosity function, mass function – galaxies: statistics.

1. Introduction

Measurements of the optical and infrared luminosity functions (LFs) and the stellar mass function (SMF) at different redshifts provide important observational tests of large scale simulations of galaxy formation and evolution. Such simulations can be either cosmological hydrodynamical models, which attempt to model the detailed physical and chemical processes involved in galaxy formation, such as ILLUSTRIS (Vogelsberger et al. 2014) and EAGLE (Schaye et al. 2015), or semi-analytic models (SAMs, e.g., Croton et al. 2006; Guo & White 2008; Lacey et al. 2016). SAMs include simple empirical representations of physical processes, and these are “added onto” the dark matter merger trees resulting from hierarchical N -body simulations (e.g., the Millennium Simulation, Springel et al. 2005). Both types of simulation make predictions of LF and SMF evolution that can be tested against observational measurements. Discrepancies between observations and simulations then provide the motivation for refining the models incorporated in the simulations. In this way, measurements of optical and infrared LF evolution have in the past motivated significant improvements in our understanding of the physical processes occurring in galaxy formation and evolution (e.g., Croton et al. 2006; Lacey et al. 2016).

As benchmarks for testing and calibrating simulations, LFs have the advantage over SMFs that they have only limited model dependencies. SMFs require the determination of stellar masses from photometry, and this involves the use of a number of physical models, notably stellar population synthesis (SPS) models (e.g., Fioc & Rocca-Volmerange 1997; Bruzual & Charlot 2003; Maraston 2005), stellar initial mass functions (IMFs; e.g., Salpeter 1955; Kennicutt 1983; Chabrier 2003),

and dust attenuation laws (e.g., Calzetti et al. 2000). SMFs are therefore subject to significant model uncertainties in addition to the observational uncertainties inherent in LFs.

Tables 1 and 2 (respectively) summarise several recent measurements of the near-infrared LF and the SMF and their evolution. Note that different studies have differentiated quiescent and star-forming galaxies in different ways (e.g., by color, morphology, or emission line strengths). Also included in these tables are low redshift ($z \leq 0.2$) studies that provide an accurate low redshift “anchor” for evolutionary studies.

A number of the studies in Table 2 derived SMFs by fitting theoretical SPS models to available photometry—for example, the *kcorrect* software of Blanton & Roweis (2007), which fits observed photometry with combinations of five template SEDs that are derived from several hundred SPS models. Others used stellar mass-to-light M/L ratios given as a function of observed color (e.g., Bell et al. 2003; Taylor et al. 2011) or redshift for red/quiescent and blue/active galaxies (e.g., Arnouts et al. 2007). It should be noted that empirical M/L ratios are also derived with the aid of SPS models.

Near-infrared (especially K -band) M/L ratios have often been preferred to optical ones for determining stellar masses because they are a much weaker function of stellar population color than optical ones. For example, Bell & de Jong (2001) found that K -band M/L ratios among spiral galaxies varied by a factor of ~ 2 , while those in the B -band varied by a factor of ~ 7 . In this work we base our measurements of SMF evolution on stellar masses calculated using M/L_K given as a function of $(B-V)$ color. Both the LF and the SMF can be approximated by Schechter (1976) functions, although the faint-end power-law index is poorly constrained when survey magnitude limits

Table 1
Some Previous Measurements of the Near-Infrared Luminosity Function and Its Evolution

References	Surveys Used	Approx. Redshift range	Redshift Type ^a (s or p)	LF Wavebands	Approx Faint limit (AB) ^b	Sample Size	Approx. Sample Area (deg ²)	Subsamples
LOW REDSHIFT STUDIES								
Loveday (2000)	Cerro Tololo 1.5 m	<0.04	s	<i>K</i>	<i>K</i> = 13.8	345	4 270	ELG/non ELG ^c
Kochanek et al. (2001)	2MASS	<0.04	s	<i>K</i>	<i>K</i> = 13.1	3 878	6 960	morphology
Cole et al. (2001)	2MASS, 2dFGRS	<0.04	s	<i>J, K</i>	<i>K</i> = 15	5 683	619	...
Bell et al. (2003)	2MASS, SDSS	< <i>z</i> > = 0.078	s	<i>ugrizK</i>	<i>K</i> = 15.3	6 282	414	morphology, color
Huang et al. (2003)	Hawaii+AAO K-band GRS	< <i>z</i> > = 0.136	s	<i>K</i>	<i>K</i> = 16.8	1 056	8.22	morphology
Eke et al. (2005)	2MASS, 2dFGRS	<0.12	s	<i>J, K</i>	<i>K</i> = 15.2	15 664	–	cluster or group size
Jones et al. (2006)	6dFGS	0.054	s	<i>b_{JrJHK}</i>	<i>K</i> = 14.6	60 869	9 075	...
Devereux et al. (2009)	2MASS	<0.01	s	<i>K</i>	<i>K</i> = 11.8	1 613	~15 000	morphology
Smith et al. (2009)	UKIDSS, SDSS	0.01 < <i>z</i> < 0.3	s	<i>r, K</i>	<i>K</i> = 17.8	40 111	619	color
Hill et al. (2010)	MGC, UKIDSS, SDSS	<0.1	s	<i>ugrizYJHK</i>	<i>K</i> = 17.5	1 785	28	...
Driver et al. (2012)	GAMA, GALEX, SDSS, UKIDSS	<0.1	s	FUV, NUV, <i>ugrizYJHK</i>	<i>K</i> = 19.9	7 638	125	morphology
Kelvin et al. (2014)	GAMA	0.025 < <i>z</i> < 0.06	s	<i>ugrizYJHK</i>	<i>r</i> = 19.4	3 727	144	morphology
Bonne et al. (2015)	2MASS	<0.05	p	<i>K</i>	<i>K</i> = 12.6	13 325	all but GP ^d	morphology, color
STUDIES OF LF EVOLUTION								
Drory et al. (2003)	MUNICS	0.4 < <i>z</i> < 1.2	p	<i>K</i>	<i>K</i> = 21.3	~5 000	0.28	...
Pozzetti et al. (2003)	K20	<i>z</i> = 0.5, 1.0, 1.5	s	<i>J, K</i>	<i>K</i> = 21.8	489	0.014	ELG/non ELG ^c
Cirasuolo et al. (2007)	UKIDSS UDS	0.25 < <i>z</i> < 2.25	p	<i>K</i>	<i>K</i> = 22.5	22 000	0.6	color
Arnouts et al. (2007)	SWIRE, VVDS, CFHTLS, UKIDSS UDS	0.2 < <i>z</i> < 2.0	p	<i>K</i>	<i>K</i> = 22.0	21 200	0.76	SED fits
Cirasuolo et al. (2010)	UKIDSS UDS, SXDS	0.2 < <i>z</i> < 4.0	p	<i>K</i>	<i>K</i> = 23	~50 000	0.7	...
Mortlock et al. (2017)	UltraVISTA, CANDELS, HUDF	0.25 < <i>z</i> < 3.75	p	<i>K</i>	<i>K</i> = 22.8	88 484	1.0	...
This work	NDWFS, SDWFS, NEWFIRM	0.2 < <i>z</i> < 1.2	p	<i>K</i>	<i>I</i> = 24, [3.6 μm] = 23.3	359 802	8.26	color

Notes.^a Spectroscopic (s) or photometric (p) redshifts.^b These faint limits are only intended to provide approximate depth comparisons between different surveys, as different authors quote survey depths to different completeness (typically 5σ).^c ELG = emission line galaxy.^d GP = Galactic plane.

are close to the characteristic magnitude or log stellar mass (M_K^* or $\log_{10} M^*$ respectively). Given the steep faint-end slope for star-forming galaxies, uncertainty in the power-law index has a significant impact on estimates of the luminosity and mass densities of these galaxies.

There is general agreement in the literature that the evolution of quiescent stellar mass density (SMD) has been more rapid than that of star-forming SMD (e.g., Brammer et al. 2011; Moustakas et al. 2013; Muzzin et al. 2013; Tomczak et al. 2014). There is agreement that the rate of increase of the space density of quiescent galaxies has depended strongly on galaxy mass, with smaller galaxies increasing more rapidly in numbers than larger ones (e.g., Muzzin et al. 2013). The most massive quiescent galaxies have increased relatively slowly in stellar mass, implying that most of their stellar mass was already in

place at higher redshift with very little stellar mass added (e.g., Brown et al. 2007; Moustakas et al. 2013; Muzzin et al. 2013).

In this study, we have provided precise measurements of the evolution of the *K*-band LF and the galaxy SMF between $z = 0.2$ and $z = 1.2$. Our very large sample of 353,594 galaxies spanning an area of 8.26 deg² in Boötes enabled us to significantly reduce Poisson errors and the effects of cosmic variance. The significant depth $I = 24.0$ of our survey allowed us to measure precisely the evolution of red and blue galaxies, both combined and separately, from $z = 1.2$. For this work, we used the low redshift Kochanek et al. (2001) LF and the Cole et al. (2001) SMF as $z \sim 0$ reference points.

We have employed the same data and similar methods to those that Beare et al. (2015) used to measure optical *B*-band LF evolution over the redshift range $0.2 < z < 1.2$. We used

Table 2
Some Previous Measurements of the Stellar Mass Function and Its Evolution

References	Surveys	Approx.	Redshift	Approx	Sample	Approx. Sample Area (deg ²)	Subsamples	Stellar Mass Based on
	Used	Redshift Range	Type ^a (s or p)	Faint Limit (AB) ^b	Size			
LOW REDSHIFT STUDIES								
Cole et al. (2001)	2MASS, 2dFGRS	<0.04	s	$K = 13.1$	5 683	6 19	...	SED fit
Bell et al. (2003)	2MASS, SDSS	$< z > = 0.078$	s	$r = 17.5,$ $K = 13.5$	18 714	414	concn. index, color	$M/L_g,$ M/L_K
Eke et al. (2005)	2MASS, 2dFGRS	< 0.12	s	$K = 15.2$	15 664	...	cluster or group size	SED fit
Li & White (2009)	SDSS	$0.001 < z < 0.5$	s	$r = 17.6$	486 840	6 437	...	kcorrect
Smith et al. (2009)	UKIDSS, SDSS	$0.01 < z < 0.3$	s	$K = 20.1$	40 111	6 19	color	kcorrect
Baldry et al. (2012)	GAMA	$0.002 < z < 0.06$	s	$r = 19.8$	5 210	143	...	M/L_i
STUDIES OF SMF EVOLUTION								
Drory et al. (2005)	GOODS-S, FORS	< 0.5	p	$I = 26.8,$ $K = 25.4$	5 557, 3 367	0.025	...	SED fit
Arnouts et al. (2007)	SWIRE, VVDS, CFHTLS, UKIDSS UDS	$0.2 < z < 2.0$	p	$[3.6 \mu\text{m}]$ $=21.5$	$\sim 21\,200$	0.76	SED fits	M/L_K
Bundy et al. (2006)	DEEP2 Palomar NIR	$0.4 < z < 1.4$	s	$K = 21.5$	$\sim 8\,000$	1.5	morphology, color, ELW	M/L_K
Borch et al. (2006)	COMBO17	$0.2 < z < 1.0$	p	$R = 24$	$\sim 25\,000$	0.78	color	M/L by SED fit
Pérez-González et al. (2008)	IRAC, MIPS, Subaru, other optical + IR	$0.0 < z < 4.0$	p	$[3.6 \mu\text{m}]$ $=23.4$	28 000	0.18	SFR	SED fit for $[3.6 \mu\text{m}]$
Drory et al. (2009)	COSMOS	$0.2 < z < 1.0$	p	$i^+ = 25,$ $K = 24$	138 001	1.73	SED fits, color	SED fit
Ilbert et al. (2010)	COSMOS	$0.2 < z < 2.0$	p	$[3.6 \mu\text{m}]$ $=23.9$	196 000	2.3	morphology, color	M/L by SED fit
Brammer et al. (2011)	NEWFIRM MBS	$0.4 < z < 2.2$	p	$K = 22.8$	$\sim 27\,000$	0.39	color	SED fit
González et al. (2011)	IRAC, <i>HST</i> ACS, <i>HST</i> WFC3/IR	$4 < z < 7$	p	$J \sim 28$	437	0.011	...	SED fit
Mortlock et al. (2011)	<i>HST</i> NICMOS	$1.0 < z < 3.5$	p	$H = 26.8$	8 298	0.73	color, SFR	SED fit
Ilbert et al. (2013)	UltraVISTA	$0.2 < z < 4.0$	p	$K = 24$	220 000	1.52	color, SFR	SED fit
Moustakas et al. (2013)	PRIMUS (+SDSS)	$0 < z < 1.0$	s	$i = 23$	40 430	5.5	SFR	SED fit
Muzzin et al. (2013)	UltraVISTA	$0 < z < 4.0$	p	$K_s = 23.4$	26 000	1.62	color	SED fit
Maraston et al. (2013)	BOSS	$0.2 < z < 0.7$	s	$r = 17.6$	$\sim 400\,000$ (massive only)	3275	...	SED fit
Davidzon et al. (2013)	VIPERS (+CFHT, <i>GALEX</i>)	$0.5 < z < 1.3$	s	$i = 22.5$	53 608	10.31	color	SED fit
Tomczak et al. (2014)	ZFOURGE/ CANDELS	$0.2 < z < 3.0$	p	$K \sim 25$	76 505	0.09	color	SED fit
This work	NDWFS, SDWFS, NEWFIRM	$0.2 < z < 1.2$	p	$I = 24,$ $[3.6 \mu\text{m}]$ $=23.3$	359 802	8.26	color	M/L_K

Notes.^a Spectroscopic (s) or photometric (p) redshifts.^b These faint limits are only intended to provide approximate depth comparisons between different surveys, as different authors quote survey depths to different completeness (typically 5σ).

the same optical and near-infrared photometry, our apparent magnitudes and colors were based on the same measurements of total flux, and we used the same method of calculating absolute magnitudes (Beare et al. 2014). For this paper, we have used improved photometric redshifts,

employing the Bayesian EAZY code to match our photometry to the 129 empirical galaxy templates of Brown et al. (2014).

The structure of this paper is as follows. Section 2 describes our imaging and catalogs. Section 3 provides our photometric redshifts. Sections 4 and 5 show how we measured galaxy

luminosities and stellar masses, and Section 6 is our sample selection. Sections 7 and 8 describe how we measured evolution of the K -band LF and the SMF. Sections 9 and 10 present our results for evolution of K -band luminosities and stellar masses and discuss their significance. Finally, we summarize our work and conclusions in Section 11.

Our results were determined assuming a cosmology⁴ with $\Omega_0 = 0.3$, $\Omega_k = 0$, $H_0 = 70 \text{ km s}^{-1} \text{ Mpc}^{-1}$, which is similar to that measured by *Wilkinson Microwave Anisotropy Probe* (Bennett et al. 2013), and presented using AB-based magnitudes and units in which $h_{70} = H_0/70$.

2. Imaging and Catalogs

The images, catalogs, and photometry were identical to those used in Beare et al. (2015). They provided a very large sample of 353 594 galaxies covering a substantial area of 8.26 deg^2 in Boötes, surveyed to a depth of $I = 24.0$. Our sample was excellent for measuring LF and SMF evolution because it was deep enough to provide precise photometry out to $z = 1.2$. and because its large size minimized random (Poisson) error and the effects of cosmic variance. Furthermore, we were able to utilize photometry in 13 optical and near-infrared wavebands, and this enabled us to obtain precise photometric redshifts, to calculate precise K -corrections (Beare et al. 2014) for determining rest-frame magnitudes and colors, and to apply cuts to exclude stars and AGN. Here we provide only a brief summary of our data. We refer the reader to Beare et al. (2015) for a more thorough description.

We used an update of the galaxy catalog produced by Brown et al. (2007), which includes additional images, photometry, and minor refinements to the photometry code. Brown et al. (2007) detected sources in the Boötes field using SExtractor 2.3.2 (Bertin & Arnouts 1996), run on I -band images from the NWDFS third data release. They removed regions surrounding very extended galaxies and saturated stars in order to minimize contamination and the final sample covered an area of 8.26 deg^2 over a 2.9×3.6 field of view.

Optical photometry was based on B_{WRI} -band imaging from the NOAO Deep Wide Field Survey (NDWFS, Jannuzi & Dey 1999). Near-infrared photometry was derived from J , H , and K_s -band imaging from the NEWFIRM Boötes Imaging Survey (A. H. Gonzalez et al. 2011, in preparation); u - and y -band images were from the $2 \times 8.4 \text{ m}$ Large Binocular Telescope (LBT; Bian et al. 2013); z -band data were from the 8.2 m Subaru Telescope (Miyazaki et al. 2012); and 3.6 , 4.5 , 5.8 , and $8.0 \mu\text{m}$ imaging was from the IRAC camera of the Spitzer Deep Wide Field Survey (SDWFS; Ashby et al. 2009; Eisenhardt et al. 2008).

We used the method described in Beare et al. (2015) to measure the total flux from each galaxy. This employs magnitude-dependent aperture sizes and applies corrections based on growth curves of apparent magnitude with aperture size to precisely account for flux falling outside the photometric aperture.

3. Determining Photometric Redshifts

Measurements of galaxy distances, and hence rest-frame magnitudes, rely on accurate redshifts. For the Boötes field, we had to rely on photometric redshifts for the vast

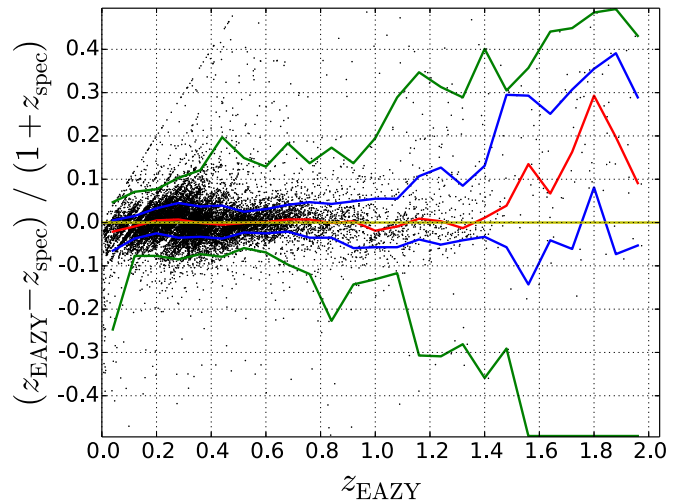


Figure 1. Fractional errors $(z_{\text{phot}} - z_{\text{spec}})/(1 + z_{\text{phot}})$ in our Bayesian photometric redshifts, as calculated using EAZY. The systematic (median) error is shown by the red line. A total of 68% of errors appear between the whole 1σ lines, and 95% of errors are between the green 2σ lines. Across the redshift range, random errors are less than ~ 0.05 , while systematic errors are less than 0.01 at $0.2 < z_{\text{phot}} < 1.0$ and less than 0.02 at $1.0 < z_{\text{phot}} < 1.2$.

majority of our galaxies, as spectroscopic redshifts were only available for 3.4% of galaxies in the redshift range $0.2 \leq z \leq 1.2$ (12 191 in all). Our photometric redshifts were determined using the Bayesian EAZY code (Brammer et al. 2008; Taylor et al. 2009) to model photometry in 13 optical to near-infrared wavebands using the 129 empirical template SEDs from Brown et al. (2014). Figure 1 shows that our photometric redshifts have $(z_{\text{phot}} - z_{\text{spec}})/(1 + z_{\text{spec}})$ systematic errors of less than 0.01 at $z_{\text{phot}} < 1.0$, while at $1.0 < z_{\text{phot}} < 1.2$ the systematic errors are less than 0.02. Our 1σ random errors were less than ~ 0.05 over the whole of our redshift range. The percentage of catastrophic errors, defined using the $|z_{\text{phot}} - z_{\text{spec}}|/(1 + z_{\text{spec}}) > 0.15$ criterion of Ilbert et al. (2013), was 1.50 (0.75, 2.17)% for all (red, blue) galaxies.

We chose to use Bayesian photometric redshifts because these do not exhibit the significant aliasing or bunching at specific redshifts seen in photometric redshifts based on frequentist least-squares fitting (as in Beare et al. 2015). Both sets of photometric redshifts exhibit similar systematic and random errors, but the even distribution of the Bayesian redshifts ensures that bunching around preferred values does not affect the numbers of galaxies allocated to different redshift bins.

When available, we used spectroscopic redshifts in place of photometric redshifts. These were mainly from the AGN and Galaxy Evolution Survey (AGES, Kochanek et al. 2012), with several hundred additional redshifts from SDSS and a variety of programmes with the Gemini, Keck, and Kitt Peak National Observatory telescopes.

4. Measuring Absolute Magnitudes

In order to measure evolution of the K -band LF, we first used the method of Beare et al. (2014) to determine the absolute magnitudes of our galaxies. This method enables the absolute magnitude M_W in a waveband W to be precisely measured using a single, carefully chosen, observed color ($m_Y - m_Z$) and apparent magnitude m_Z . As Figure 2 shows, M_W is determined from the second degree polynomial best fit to a

⁴ Conversions to other cosmologies can be made as described in Croton (2013).

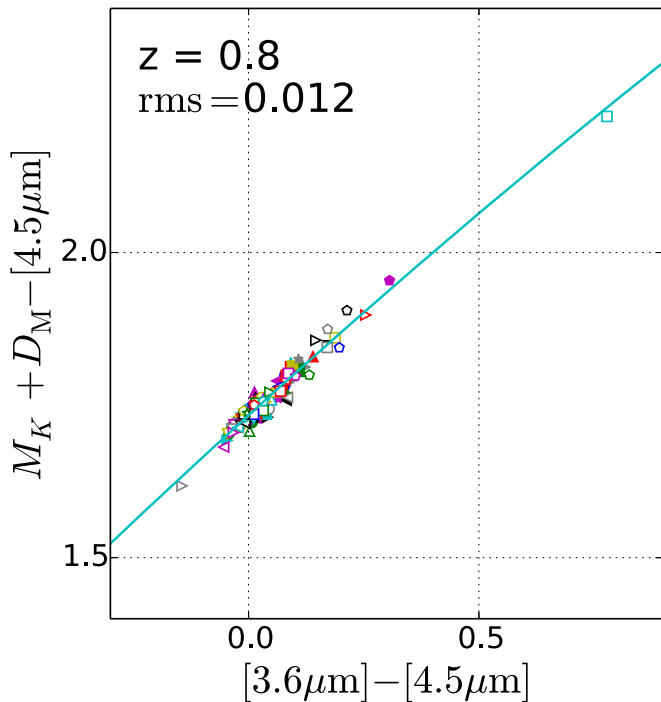


Figure 2. Example plot showing how we determined absolute magnitudes from observed colors using the method of Beare et al. (2014). The colored markers plot computed values of $(M_K + D_M) - [4.5 \mu\text{m}]$ against $[3.6 \mu\text{m}] - [4.5 \mu\text{m}]$ for the 129 template SEDs from Brown et al. (2014) at $z = 0.8$. D_M is the distance modulus. The curve is the best-fit second-order polynomial to the template data points and enables absolute magnitudes M_K to be determined from apparent $[3.6 \mu\text{m}]$ and $[4.5 \mu\text{m}]$ magnitudes. The rms offset from the template points is shown in the top left corner. Outliers offset by more than 0.2 mag from the polynomials were excluded from the polynomial fitting.

plot of $(M_W + D_M) - m_Z$ against $(m_Y - m_Z)$ for the 129 template galaxies of Brown et al. (2014), with D_M being the distance modulus:

$$(M_W + D_M) - m_Z = a(m_Y - m_Z)^2 + b(m_Y - m_Z) + c. \quad (1)$$

Table 3 lists the observed colors we used at different redshifts to determine absolute magnitudes in different rest-frame wavebands. The method allows precise determination of the uncertainties due to photometric error, redshift error, and intrinsic galaxy variability. (The Y - and Z -band filter transmission functions we used took account of atmospheric absorption, but the W -band rest-frame filter did not.)

We used the same method to determine absolute magnitudes in the B - and V -bands, as these were needed for calculating galaxy masses based on stellar mass-to-light ratios given as a function of rest-frame $(B - V)$ color.

The template galaxy substantially redder in $([3.6 \mu\text{m}] - [4.5 \mu\text{m}])$ color than the others in Figure 2 is the ultra-luminous infrared galaxy UGC 5101. This exhibits substantial emission from hot (\sim a few 100 K) dust in the near-infrared, indicating the presence of a powerful AGN. This outlier breaks the assumption that infrared light from galaxies is always dominated by stellar emission. However, it does in fact play a useful role in “anchoring” the polynomial used to determine absolute K -band magnitudes, preventing it from being poorly constrained.

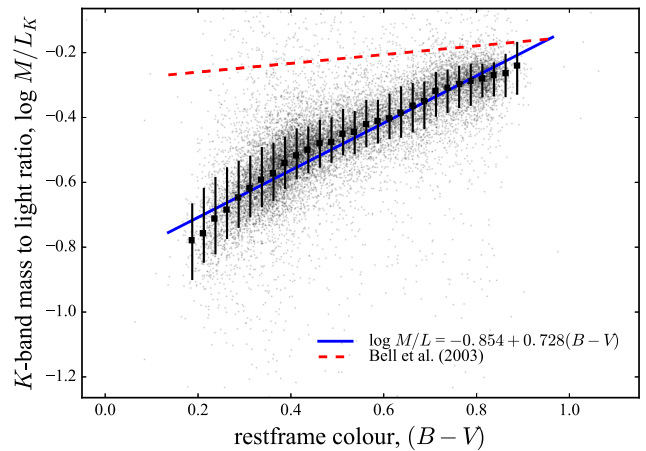


Figure 3. Stellar mass-to-light ratios for $z < 0.4$ GAMA galaxies. The gray points represent individual galaxies in the GAMA sample. Biweight means for $\log_{10} M/L_K$ in narrow bins of $(M_B - M_V)$ rest-frame color are shown by the large data points with error bars. The blue line is a best fit to these means as a function of color. The dashed red line shows the relationship from Bell et al. (2003), which overestimates galaxy masses relative to the more recent relationship based on GAMA galaxies.

Table 3
Observed Colors Used to Determine Absolute Magnitudes

Rest-frame Waveband	Effective Wavelength μm	Redshift Range	Color $(m_Y - m_Z)$
U^a	0.361	0.0 to 0.8	$B_w - R$
U^a	0.361	0.8 to 1.2	$R - I$
B	0.441	0.0 to 0.4	$B_w - I$
B	0.441	0.4 to 1.2	$R - J$
V	0.551	0.2 to 0.4	$R - K_s$
V	0.551	0.4 to 1.2	$I - J$
K	2.195	0.2 to 0.6	$K_s - [3.6 \mu\text{m}]$
K	2.195	0.6 to 1.0	$[3.6 \mu\text{m}] - [4.5 \mu\text{m}]$
K	2.195	1.0 to 1.2	$J - [4.5 \mu\text{m}]$

Notes. Absolute magnitudes in a waveband W were calculated using the method of Beare et al. (2014). Given two suitably chosen observed magnitudes m_Y and m_Z , $(M_W - m_Z)$ is given by a second-degree polynomial in the color $(m_Y - m_Z)$.

^a As calculated in Beare et al. (2015).

5. Measuring Galaxy Stellar Masses

Taylor et al. (2011) showed that optical and near-infrared stellar mass-to-light ratios (M/L) can be determined to within 0.2 dex using a linear function of a single rest-frame color. For example, Figure 3 for GAMA galaxies shows how M/L_K can be determined from rest-frame $(B - V)$ color using the following relation (in Solar units):

$$\log_{10}(M/L_K) = -0.854 + 0.728(M_B - M_V). \quad (2)$$

Determining stellar masses from color dependent mass-to-light ratios is simpler than determining them from detailed SPS modeling of individual galaxies. However, it must be remembered that relationships such as Equation (2) are derived by averaging the results of detailed SPS modeling and consequently

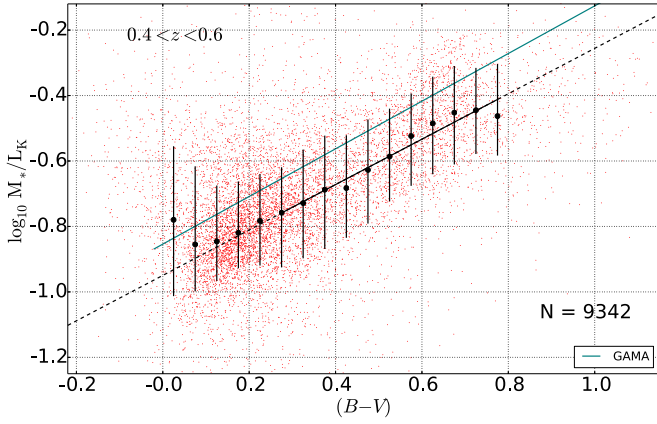


Figure 4. Example plot for G10 galaxies of $\log_{10}(M/L_K)$ against rest-frame $(B-V)$ color for one redshift bin. Galaxies are shown by red points. Median values of $\log_{10}(M/L_K)$ in color bins of width 0.5 mag are shown by filled circles and the 1σ errors by vertical bars. The linear best fit to the median $\log_{10}(M/L_K)$ values for colors between 0.3 and 0.7 is shown by the thick slanting line (extended beyond this range by dashed line). For comparison, the thin sloping green line shows the non-evolving $z < 0.4$ GAMA relationship (Equation (2)).

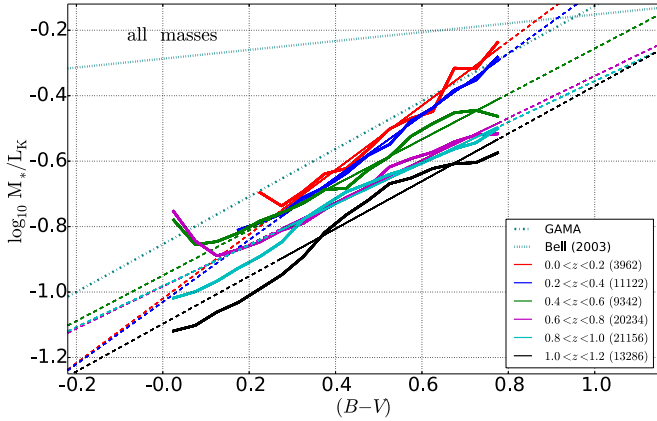


Figure 5. Median values of $\log_{10}(M/L_K)$ for G10 galaxies plotted against rest-frame $(B-V)$ color for redshifts in bins of width 0.2 mag between $z = 0$ and $z = 1.2$. Linear best fits to the median $\log_{10}(M/L_K)$ values for colors between 0.3 and 0.7 are shown by thick slanting lines (extended beyond this range by dashed lines). For comparison, the thin sloping green dotted-dashed and dotted lines show the non-evolving $z < 0.4$ GAMA and $z < 0.2$ (Bell et al. 2003) relationships, respectively.

suffer from similar problems, while at the same time increasing uncertainty as a result of the loss of detailed color information.

The stellar masses in Figure 3 were derived using Bruzual & Charlot (2003) SPS models fitted to *ugrizYJHK* optical to near-infrared photometry. The advantage of a relation such as Equation (2) over full SED fitting is that photometry is required in many fewer wavebands—in this case just those required to compute the absolute magnitudes M_B and M_V using K-corrections (Equation (1)).

Galaxies in the $z < 0.4$ GAMA survey have redshifts with a median value of 0.2 (Taylor et al. 2011), and evolution of the relation Equation (2) is not apparent in the data. However, our data extend to $z = 1.2$, and it cannot be assumed that evolution of $\log_{10}(M/L_K)$ as a function of rest-frame $(B-V)$ is not significant over this larger redshift range. Indeed, the SFHs of the stellar populations that lead to Equation (2) at $z \sim 0.2$ may not be the same as those of a comparable sample at $z \sim 1.2$, so some evolution in Equation (2) is to be expected.

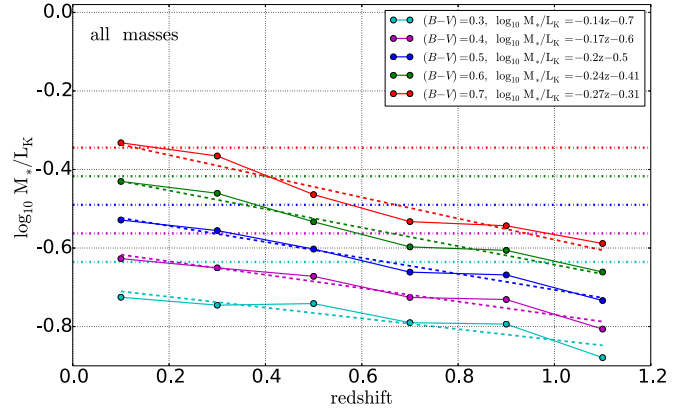


Figure 6. Evolution of the best-fit values of $\log_{10}(M/L_K)$ in Figure 5 for G10 galaxies with $(B-V)$ rest-frame colors of 0.3, 0.4, 0.5, 0.6, and 0.7. Linear best fits are shown by dashed lines, and their equations are given on the upper right. These equations can all be summarized to within 0.01 dex by the single Equation (3): $\log_{10}(M/L_K) = -[0.05 + 0.3(M_B - M_V)]z + (M_B - M_V) - 1.0$. This enables evolving mass-to-light ratios to be computed simply from redshifts and rest-frame colors. For comparison, the horizontal dashed-dotted lines show the non-evolving $z < 0.4$ GAMA relationship (Equation (2)).

We therefore endeavored to measure the evolution of the dependence of $\log_{10}(M/L_K)$ on $(B-V)$ using the G10 catalog, which contains consistent total flux measurements across 38 far-UV to far-IR for sources in a 1 deg^2 subset of the COSMOS region (Davies et al. 2015; Andrews et al. 2017). The G10 catalog employed the LAMBDAAR code (Wright et al. 2016) to largely eliminate systematic error arising from the different flux measurements and reduction methods used by constituent COSMOS surveys. It aimed to produce a catalog extending to $z = 1$, which was consistent with the low redshift ($z < 0.4$) spectroscopic GAMA survey (Driver et al. 2011; Liske et al. 2015).

Stellar masses for galaxies in the G10 catalog were calculated using MAGPHYS (da Cunha et al. 2008). As shown by the example in Figure 4, for each redshift bin, we plotted G10 values of $\log_{10}(M/L_K)$ and 1σ deviations against rest-frame $(B-V)$ color, and determined the median y-axis values of $\log_{10}(M/L_K)$ for different color bins on the x-axis (solid points and vertical bars).

We performed a linear best fit to the median $\log_{10}(M/L_K)$ values for colors in the range 0.3 to 0.7. Figure 5 shows how these median $\log_{10}(M/L_K)$ values and best-fit relationships have evolved with redshift.

To measure the evolution of $\log_{10}(M/L_K)$ as a function of rest-frame color, the best fit median $\log_{10}(M/L_K)$ values corresponding to $(B-V)$ colors of 0.3, 0.4, 0.5, 0.6, and 0.7 were plotted against redshift, as in Figure 6. (Each curve in this plot corresponds to the intersections of a vertical line of constant color with the best-fit lines in the preceding plot.)

Equations for the linear best fits to the five plots in Figure 6 are shown in the top right-hand corner. It turns out that they can all be described to within 0.01 dex by just one function of $(B-V)$ and redshift:

$$\log_{10}(M/L_K) = -[0.05 + 0.30(M_B - M_V)] \times z + (M_B - M_V) - 1.00. \quad (3)$$

We derived Equation (3) using $(B-V)$ colors between 0.3 and 0.7, because a primary focus of this paper is to study evolution of the stellar mass in red galaxies and this rest-frame color range is sufficient to encompass all red sequence galaxies

at $z < 1.2$. Also, a close linear fit was apparent for colors between 0.3 and 0.7, random error being ~ 0.2 dex and systematic error being up to ~ 0.03 dex. For galaxies bluer than $(B - V) = 0.3$, the random error is similar but the systematic error is greater—up to ~ 0.06 dex.

As the example plot in Figure 4 illustrates, the 1σ scatter in $\log_{10}(M/L_K)$ values for given rest-frame color is generally ~ 0.2 dex. However, some of this variation is due to random error in the G10 photometry rather than just intrinsic variability among galaxies. Taylor et al. (2011) found a smaller variation of only ~ 0.1 dex for GAMA galaxies at $z < 0.4$, as can be seen in Figure 3. We take their value $\sigma = 0.1$ dex as intrinsic scatter of $\log_{10} M_K/L$ at fixed $(B - V)$.

As Figure 5 shows, our evolving relationship, Equation (3), exhibits a broadly similar dependence on rest-frame color to the GAMA one, but it evolves at a rate that depends on color—this rate being slightly faster for red galaxies than for blue. This is more clearly seen in Figure 6.

As is clear from Figure 5, the 2MASS-based $\log_{10}(M/L_K)$ values from Bell et al. (2003) vary little with $(M_B - M_V)$ color, whereas our values and those based on GAMA are a strong function of color. Bell et al. (2003) used the observed SDSS +2MASS colors of galaxies and masses determined by SED fitting, and we suspect that the difference is due to 2MASS underestimating the fluxes of star-forming galaxies causing their M/L_K values to be greater than ours by ~ 0.4 dex for the bluest galaxies but less than ~ 0.1 dex for the reddest galaxies. When converted for a Chabrier IMF, the Bell et al. (2003) relation is

$$\log_{10}(M/L_K) = -0.287 + 0.135(M_B - M_V). \quad (4)$$

Equation (3) is based on the mean properties of an ever-changing population of red G10 galaxies—that is, a population that is continually being augmented by blue galaxies which have ceased star formation, and one in which major and minor mergers and possibly bursts of star formation are changing the demographics of the population.

By contrast, in the case of massive red galaxies, we are predominantly measuring how individual massive galaxies fade and grow via mergers. As the evolutionary history of these massive red galaxies is different from that of the majority of red galaxies, we expect their dependence of $\log_{10}(M/L_K)$ on rest-frame $(B - V)$ color to evolve differently with time. We therefore investigated this separately using a subsample with $\log_{10} M > 10.75$. This mass cutoff was chosen to ensure that a range of masses was included on both sides of the mass corresponding to the fixed space density of $\tilde{\phi} = 2.5 \times 10^{-4.0} h_{70}^3 \text{Mpc}^{-3} \text{dex}^{-1}$ that we used to measure evolution of massive galaxies (see Section 8).

At $z > 0.8$, only the reddest $(B - V > 0.6)$ massive galaxies exist in significant numbers in the G10 data to permit a reliable analysis, so we confined ourselves to studying massive red galaxies with a single rest-frame color of $(B - V) = 0.7$. For massive red galaxies, we found

$$\log_{10}(M/L_K) = -[0.11 + 0.3(M_B - M_V)] \times z + (M_B - M_V) - 0.9. \quad (5)$$

We used Equation (3) for our measurement of red galaxy SMD evolution but Equation (5) for our measurement of the evolution of the massive red galaxies ($\log_{10} M > 10.75$). As explained later in Section 8, these two measurements are based on entirely separate calculations involving Schechter function fitting with different mass ranges and different α constraints

(fixed and variable, respectively). We used only Equation (3) when measuring the evolution of red galaxy SMD, and did not treat massive red galaxies separately. To do so would have introduced a discontinuity into our stellar mass measurements, and would not in any case have affected our red galaxy SMD measurements, because the presence of a small number of massive galaxies contributes a negligible fraction to overall SMD.

We note that massive red galaxies of rest-frame color $B - V = 0.7$ evolve more rapidly in (M/L_K) (0.32 dex per unit redshift) than red galaxies of the same rest-frame color as a whole (0.26 dex per unit redshift). This is to be expected because, to some extent, new arrivals from the blue cloud start off their red sequence life with similar properties, whether they arrive at $z = 1.1$ or $z = 0.1$. We therefore expect the properties of red galaxies as a whole to evolve less rapidly than those of individual massive red galaxies that are not being “diluted” by new arrivals and affected by major mergers, and this is what we observe.

It is instructive to compare the rate of (M/L_K) evolution for individual massive red galaxies to those of Bruzual & Charlot (2003) SPS models with different metallicities and formation redshifts. For solar metallicity simple stellar populations (SSPs), the rates of evolution in M/L_K from $z = 1.2$ to $z = 0$ are -0.20 , -0.24 , and -0.51 dex per unit redshift for formation redshifts $z_f = 10.0$, 4.1, and 1.4, respectively.

From Equation (5), calculated rates of evolution of $\log_{10}(M/L_K)$ for individual galaxies depend on redshift and the evolving rest-frame $(B - V)$ color. If we assume reddening of 0.1 mag per unit redshift for the most luminous red galaxies, as observed in our Boötes data and as predicted by SSPs, the net rate of change in $\log_{10}(M/L_K)$ is ~ -0.4 dex per unit redshift. This lies between the rates of change for solar metallicity SSPs with $z_f = 4.1$ and $z_f = 1.4$. We conclude therefore that the empirical Equation (5) is broadly consistent with the predictions of Bruzual & Charlot (2003) SSP models.

Our models of an evolving M/L_K relation that is a function of rest-frame $(B - V)$ extend the work of Taylor et al. (2011), showing M/L relations can be determined with 0.2 dex accuracy using a single rest-frame color out to $z \sim 1$. It should be mentioned that López-Sanjuan et al. (2019) reached a conflicting conclusion (i.e., that the dependence of M/L_i on rest-frame $(g - i)$ color has not evolved since $z = 1.5$).

We find in this study that it is essential to include evolution of M/L_K as a function of $(B - V)$ if our measurements of SMF evolution since $z = 1.2$ are to agree with previous studies that derive stellar masses directly from SPS modeling rather than via mass-to-light ratios. An evolving M/L_K versus $(B - V)$ relationship is also essential if our measurements of rates of red galaxy stellar mass evolution are to agree with those inferred from comparisons with passively evolving stellar populations.

6. Sample Selection

The same cuts as in Beare et al. (2015) were applied to limit the sample to objects brighter than $I = 24.0$ and $[3.6 \mu\text{m}] = 23.3$, and to exclude stars. We used the modified Stern et al. (2005) mid-infrared selection criteria that we used previously in Beare et al. (2015) to exclude AGN, with additional AGN identifications being made with SDSS and AGES spectroscopy. The AGN cuts removed less than 1% of our galaxy sample. Quiescent and star-forming galaxies were separated using the same evolving red-blue color cut in

rest-frame color–magnitude space:

$$(M_U - M_B) > 1.074 - 0.18z - 0.03(M_B + 19.4). \quad (6)$$

The final sample size for galaxies at redshifts $0.2 \leq z < 1.2$ with absolute magnitudes $-24 \leq M_B < 14$ was 353 594. The sample was 85% complete at our faint limit of $I = 24.0$ and $\simeq 100\%$ complete at $I = 21.5$. We corrected for the small degree of incompleteness over the range $21.5 < I < 24.0$.

7. Determining the K -band LF

K -band LFs were determined for red and blue galaxy subsamples separately, as well as for the total sample. In each case, galaxies in the redshift range $0.2 \leq z < 1.2$ were allocated to five redshift bins of equal width, $\Delta z = 0.2$. For each redshift bin, empirical binned LFs, $\Phi(M_K)$, were obtained by dividing the (completeness corrected) numbers of galaxies N in K -band absolute magnitude bins of width ΔM_K by the comoving volume ΔV corresponding to the given redshift range Δz (i.e., $\Phi(M_K) = N/\Delta V$).

For each redshift bin, we used the maximum likelihood method (Marshall et al. 1983) to fit Schechter (1976) functions to the (unbinned) absolute magnitude data over a magnitude range no wider than that over which the sample was complete to $I = 24.0$. This range was determined from a plot of $(M_K + D_M - I)$ against redshift. In terms of luminosities, the Schechter function is

$$\phi_K(L_K)dL_K = \left(\frac{\phi_K^*}{L_K^*}\right)\left(\frac{L_K}{L_K^*}\right)^\alpha \exp\left(\frac{-L_K}{L_K^*}\right)dL_K. \quad (7)$$

Here, ϕ_K is the comoving space density per unit increment in luminosity L_K , ϕ_K^* is a normalizing factor (the characteristic space density), L_K^* is the characteristic luminosity corresponding roughly to the transition from a power-law LF to an exponential one, and α determines the slope of the power-law variation at the faint end. The characteristic space density ϕ_K^* provides an approximate measure of the space density close to the characteristic magnitude (more specifically $\phi_K = 1.086\phi_K^*$ at $M_K = M_K^*$). The maximum likelihood method provides an estimate of Schechter fit parameter uncertainties.

It is often more useful to write the Schechter function in terms of absolute magnitudes M_K :

$$\begin{aligned} \phi_K(M_K)dM_K \\ = -0.4 \ln 10 \phi_K^* 10^{-0.4(\alpha+1)(M_K - M_K^*)} \exp(-10^{-0.4(M_K - M_K^*)}) dM_K. \end{aligned} \quad (8)$$

Integrating over all luminosities gives the total luminosity density j_K in waveband K :

$$j_K = \phi_K^* L_K^* \Gamma(\alpha + 2). \quad (9)$$

Because α becomes increasingly poorly constrained as redshift increases, we kept α fixed at values corresponding to those for the lowest two redshift bins ($0.2 \leq z < 0.4$ and $0.4 \leq z < 0.6$) where α was a free parameter—namely, -0.5 , -1.2 , and -1.0 for red, blue, and all galaxies respectively.

To measure luminosity evolution of the most luminous galaxies, we determined how the rest-frame magnitude \tilde{M}_K corresponding to a fixed space density of $\tilde{\phi} = 10^{-4.0} h_{70}^3 \text{Mpc}^{-3} \text{mag}^{-1}$ had evolved. In order to do this as precisely as possible, we fitted a Schechter function with variable α parameter just to the bright end

of the LF (i.e., using only data points brighter than K -band magnitude -23.0). This procedure effectively uses the Schechter function as a convenient measuring tool, with the precise values of the Schechter parameters not having any other relevance.

8. Determining the SMF

We measured binned SMFs of red, blue, and all galaxies in the same manner as the binned LFs, including determining mass limits using the apparent magnitude limits and the mass-to-light ratios of passive galaxies. To parameterize our SMFs and measure their evolution, we used the maximum likelihood method to fit Schechter functions to the (unbinned) galaxy masses over a mass range no wider than that over which the sample was complete to $I = 24.0$:

$$\phi_M(M)dM = \left(\frac{\phi_M^*}{M^*}\right)\left(\frac{M}{M^*}\right)^\alpha \exp\left(\frac{-M}{M^*}\right)dM. \quad (10)$$

Here ϕ_M is the comoving space density per unit increment in stellar mass M , ϕ_M^* is a normalizing factor, M^* is a characteristic mass, and α determines the slope of the power-law variation at the low mass end. We used fixed α values of -0.5 , -1.2 , and -1.0 for red, blue, and all galaxies, respectively.

Given the large range of galaxy masses and to avoid confusion between mass and absolute magnitude, we rewrite Equation (10) in terms of logarithms of the mass $\mu = \log_{10}(M/M_\odot)$, so the comoving density per unit μ is

$$\phi_\mu(\mu)d\mu = (\phi_\mu^* \ln 10) 10^{(\alpha+1)(\mu-\mu^*)} \exp(-10^{(\mu-\mu^*)}) d\mu. \quad (11)$$

Here ϕ_μ^* is the normalizing factor and $\mu^* = \log_{10} M^*$. At the value $\mu = \mu^*$, $\phi = \phi^* \ln 10 = 2.30\phi^*$, so ϕ_μ^* effectively measures the space density of galaxies per unit $\mu = \log_{10} M$ at the characteristic mass M^* .

Integrating Equation (10) over all masses gives the total SMD in galaxies,

$$\rho_M = \phi^* M^* \Gamma(\alpha + 2). \quad (12)$$

To measure evolution of the mass of the most massive galaxies, we determined how the value $\log_{10} \tilde{M}$ corresponding to a fixed space density of $\tilde{\phi} = 2.5 \times 10^{-4.0} h_{70}^3 \text{Mpc}^{-3} \text{dex}^{-1}$ had evolved. In order to do this as precisely as possible, we fitted a Schechter function with variable α parameter just to the massive end of the SMF—that is, using only data points for red (blue, all) galaxies for which $\log_{10}(M/M_\odot) > 11.0$ (10.5, 10.5). (Because a luminosity ratio of 1.0 dex is equivalent to 2.5 mag, an LF space density of $10^{-4.0} h_{70}^3 \text{Mpc}^{-3} \text{mag}^{-1}$ is equivalent to an SMF space density of $\tilde{\phi} = 2.5 \times 10^{-4.0} h_{70}^3 \text{Mpc}^{-3} \text{dex}^{-1}$, assuming a fixed stellar M/L ratio. The fixed space densities used for the LF and SMF were therefore equivalent.)

9. K -band Luminosity Evolution—Results and Discussion

9.1. K -band LF Evolution—Space Density and Characteristic Magnitude

Figures 7 to 9 show our binned K -band LFs for all, red, and blue galaxies, together with results from a variety of previous studies. Our binned LFs are tabulated in Tables 7–9. Maximum likelihood fits to our (unbinned) data are overplotted as continuous red lines. To provide a fixed reference, we show the local LFs of Kochanek et al. (2001) for all, red, and blue

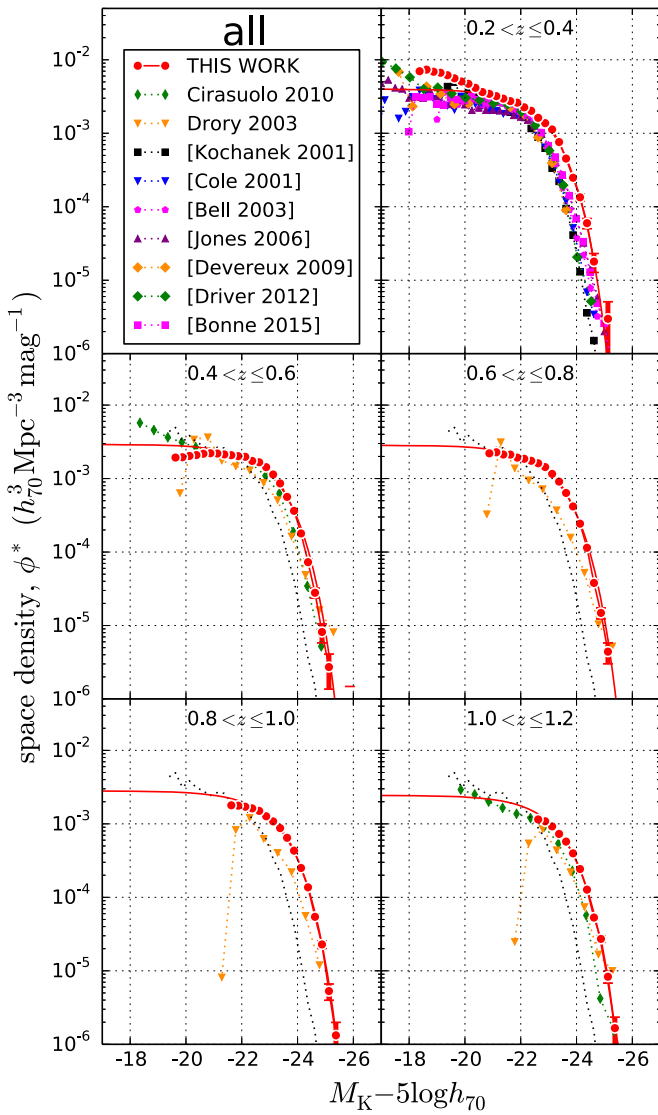


Figure 7. Binned K -band LFs for all galaxies in bins of width 0.2 mag with $1 - \sigma$ Poisson uncertainties, shown for the Boötes data. Overplotted in red are maximum likelihood fits to the (unbinned) data. LFs for the low redshift universe are labeled using square brackets. To provide a fixed reference, $z \sim 0$ results from Kochanek et al. (2001) are shown as black dotted lines in the lower four panels. Our LFs (red points) are brighter than some of the literature, with offsets of up to ~ 0.5 mag at $z \sim 0.3$.

galaxies in each bin. We only plot bins for which 97.7% (the $2 - \sigma$ limit) of the measured absolute magnitudes have observed magnitudes brighter than our faint limit of $I = 24.0$.

Our LFs are often brighter than the prior literature, with differences of up to ~ 0.5 mag evident for $z \sim 0.3$, where bright galaxies are relatively well-resolved. We attribute this to our careful accounting for light falling outside the photometric aperture by the use of magnitude dependent aperture sizes and corrections based on growth curves of measured magnitude with aperture diameter (Beare et al. 2015). Figure 10 shows more clearly the difference between our LF and those of other authors for all galaxies at $0.2 < z \leq 0.4$. (Our binned data points lie above unity for the faintest galaxies, i.e., $M_K - 5 \log h_{70} > -21$, because our maximum likelihood Schechter fit in Figure 7 underestimates the space density at fainter magnitudes.) We measure significantly greater space densities for the brightest galaxies compared to other authors.

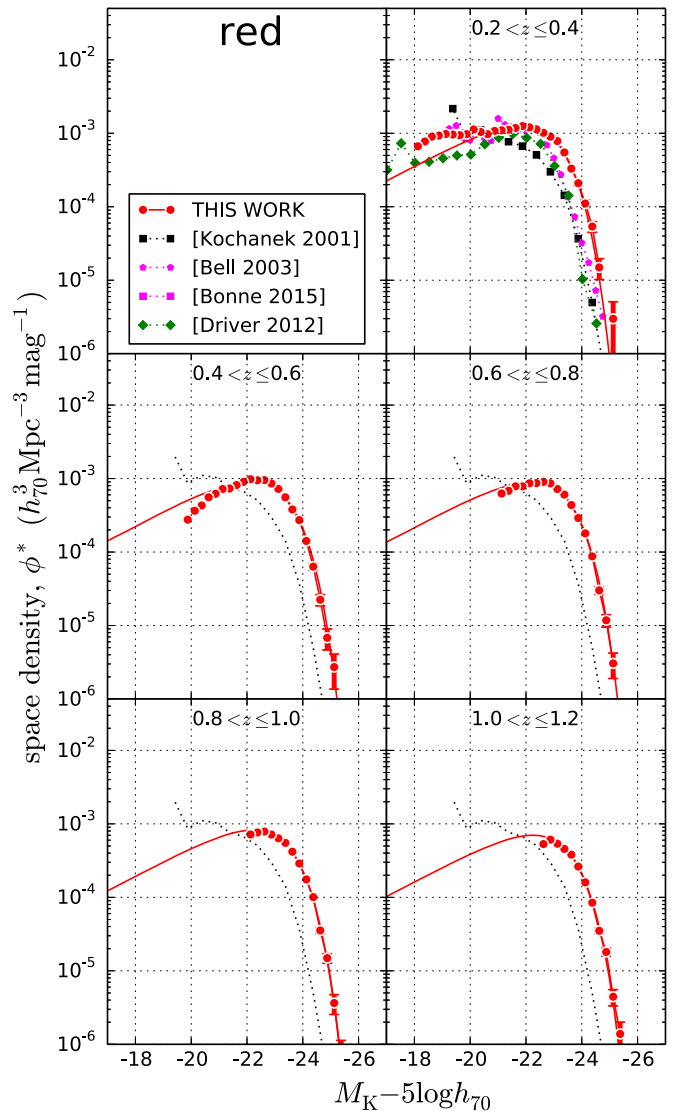


Figure 8. Binned K -band LFs for red galaxies with $1 - \sigma$ Poisson uncertainties shown for the Boötes data. Overplotted in red are maximum likelihood fits to the (unbinned) data. LFs for the low redshift universe are labeled using square brackets. To provide a fixed reference, $z \sim 0$ results from Kochanek et al. (2001) are shown as black dotted lines in the lower four panels. The luminosity of the brightest red galaxies decreases with time, but not as fast as a passively evolving population, thus indicating a steady build up of mass through minor mergers.

Figures 11 to 13 show our maximum likelihood Schechter fits (continuous lines), as well as our binned space densities (data points), with all redshift bins on a single plot to make the evolution of the LFs more apparent.

We see from Figures 14 and 15 and Table 4 that the characteristic space density ϕ_K^* approximately doubled for both red and blue galaxies from $z \sim 1.1$ to $z \sim 0.3$, while the characteristic magnitude M_K^* of red galaxies faded by ~ 0.4 mag and that of blue by ~ 0.7 mag. The more rapid fading of M_K^* for blue galaxies is consistent with downsizing (Cowie et al. 1996)—that is, the greater proportion of high mass galaxies seen in the star-forming population at $z \sim 2$ versus $z \sim 0$.

Luminosity density, as calculated by Equation (9), is a more physically meaningful quantity than the three individual Schechter parameters, because these relate to a specific functional representation of the LF rather than measurable

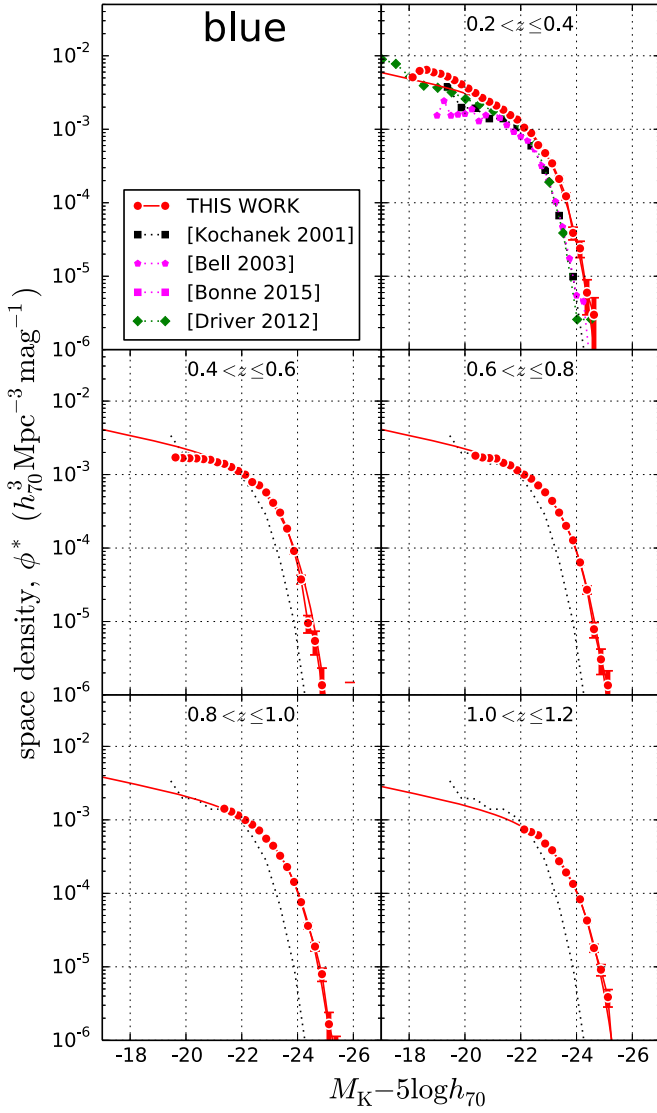


Figure 9. Binned K -band LFs for blue galaxies with $1 - \sigma$ Poisson uncertainties shown for the Boötes data. Overplotted in red are maximum likelihood fits to the (unbinned) data. LFs for the low redshift universe are labeled using square brackets. To provide a fixed reference, $z \sim 0$ results from Kochanek et al. (2001) are shown as black dotted lines in the lower four panels. The luminosity of the brightest blue galaxies decreases with time.

physical quantities. Furthermore, luminosity density is relatively insensitive to degeneracy among the three Schechter parameters, because it is effectively the luminosity weighted area under the LF. This is illustrated by the fact that Jones et al. (2006) obtained a value for ϕ_K^* for all galaxies, which is half that of Bell et al. (2003), and an α value of -1.16 as compared with -0.77 , but the two studies obtained luminosity densities within 4% of each other.

9.2. K -band Luminosity Density Evolution

Figure 16 plots evolution of the total luminosity density j_K , showing that it increased by $20\% \pm 10\%$ (0.08 dex) from $z \sim 1.1$ to $z \sim 0.3$ for all, red, and blue galaxies. Also plotted are the results of Cirasuolo et al. (2010), Arnouts et al. (2007), and Drory et al. (2003), and luminosity densities for the same six low redshift studies as in Figures 14 and 15.

For red galaxies, the measured luminosity density increase by a factor of ~ 1.2 implies a buildup of stellar mass, because a

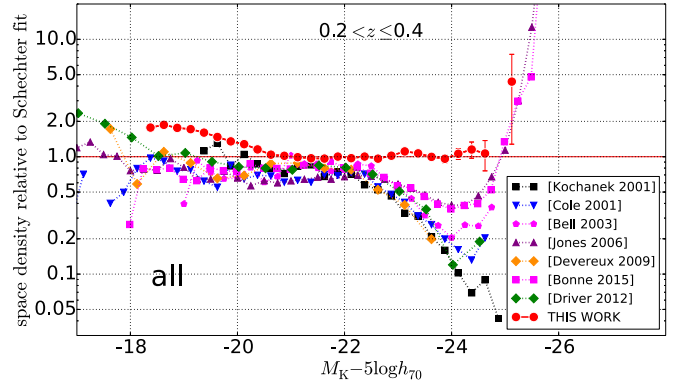


Figure 10. Detailed comparison of K -band space densities for all galaxies at $0.2 \leq z < 0.4$, with $1 - \sigma$ Poisson uncertainties shown for the Boötes data. This displays the same data as in the top right panel of Figure 7, but plotting the ratio of binned space densities from the literature to the (unbinned) maximum likelihood Schechter function fit to our data. LFs for the low redshift universe are labeled using square brackets. We see a greater number of highly luminous galaxies than other studies. Our results show smoother variation due to our large sample size and area.

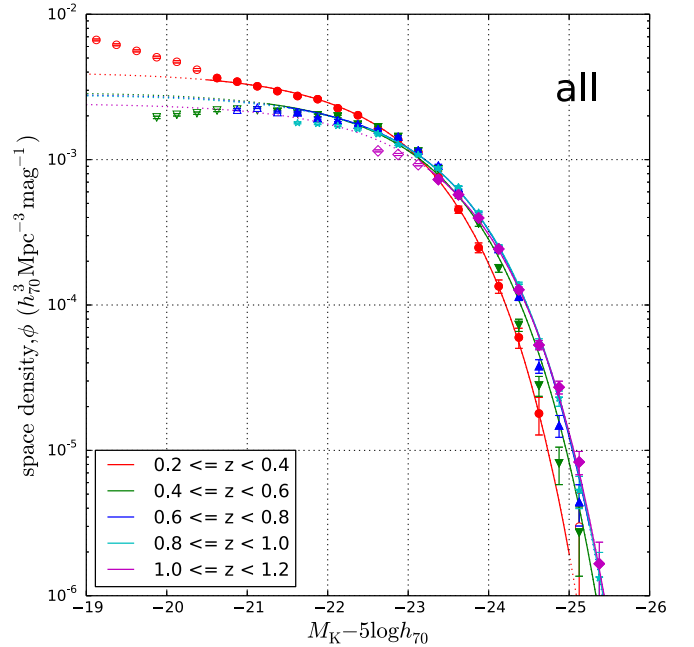


Figure 11. Evolution of the K -band Schechter function for all galaxies, showing all five redshift ranges in one panel. The symbols denote comoving space densities for the various absolute magnitude bins. Filled symbols denote the range of absolute magnitudes used to perform the maximum likelihood fit. Continuous curves show maximum likelihood fits to the (unbinned) data. Open symbols denote data for very faint galaxies that were expected to be reliable on the basis of apparent I and $[3.6 \mu\text{m}]$ magnitudes but were not represented adequately by a Schechter function. The error bars show $1 - \sigma$ Poisson uncertainties for the numbers in each bin.

passively evolving stellar population *fades* as it evolves. As in Beare et al. (2015), we estimated the increase in SMD, ρ , by comparison with a passively fading quiescent population. Taking a single burst Bruzual & Charlot (2003) SSP with formation redshift $z_f = 3.0$, solar metallicity $Z = 0.02$, and Chabrier IMF to be representative of quiescent stellar populations, evolution of the stellar mass-to-light ratio $\Upsilon = \rho/j_K$ is given by $d\Upsilon/dz = -0.24$, resulting in passive fading of ~ 0.56 mag from $z = 1.1$ to $z = 0.3$. From this, we

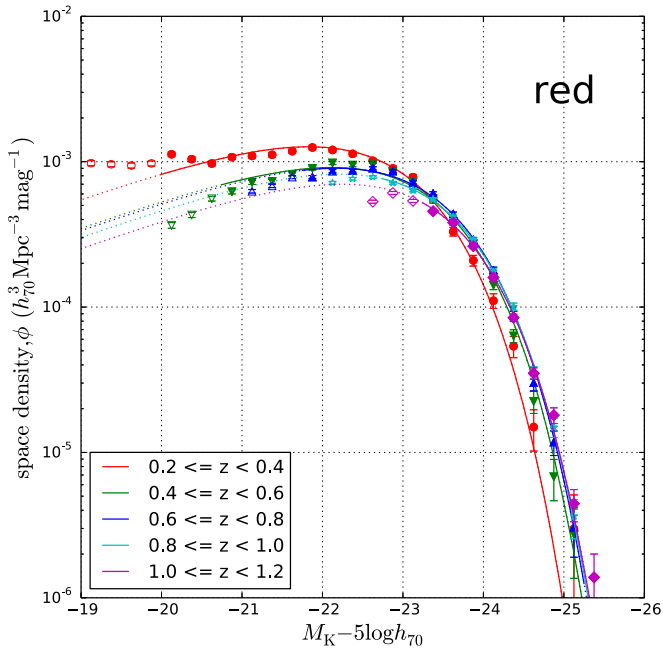


Figure 12. Evolution of the K -band Schechter function for red galaxies, showing all redshift ranges in one panel. Symbols are as in Figure 11.

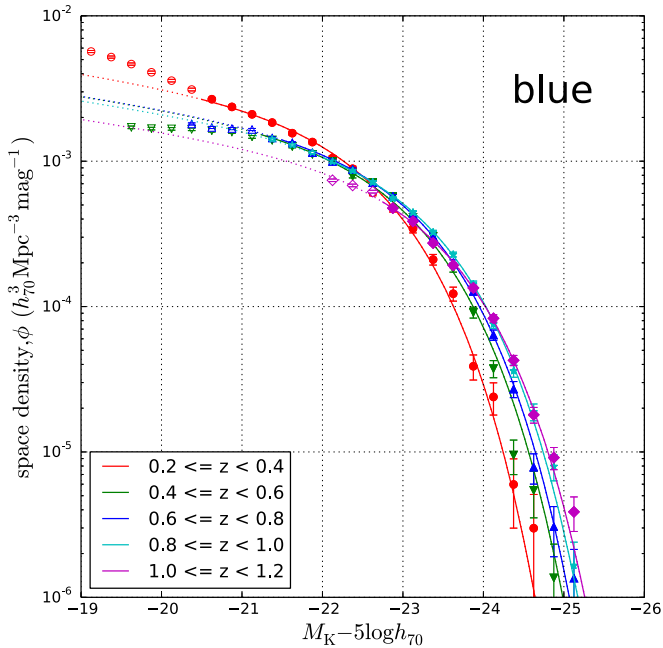


Figure 13. Evolution of the K -band Schechter function for blue galaxies, showing all redshift ranges in one panel. Symbols are as in Figure 11.

deduce that red galaxy SMD increased by a factor of ~ 2.1 from $z = 1.1$ to $z = 0.3$. Varying z_f between 4.0 and 1.5 or adopting a very low metallicity of $Z = 0.0001$ alters the measured SMD increase by less than 20%.

9.3. K -band Luminosity Evolution of Highly Luminous Galaxies

As argued by Bell et al. (2004), luminous red galaxies have evolved by a combination of passive stellar fading and the addition of stellar mass through mergers, because highly luminous blue galaxies are too rare to account for the growth in

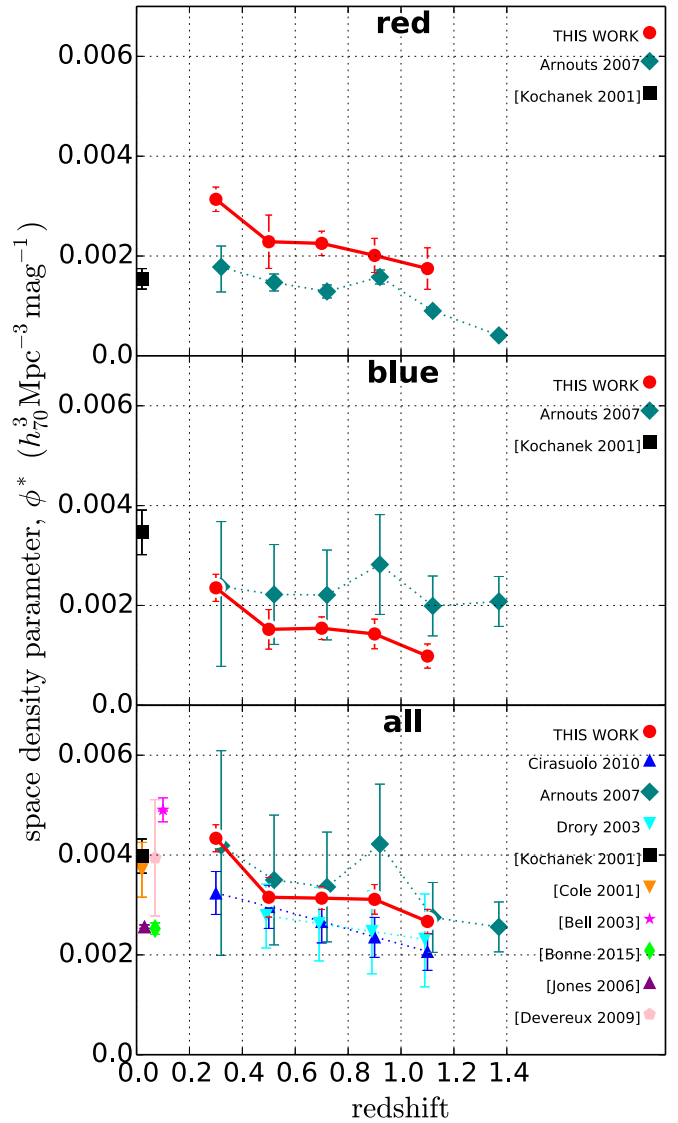


Figure 14. Evolution from $z = 1.1$ to $z = 0.3$ of the K -band maximum likelihood Schechter parameter ϕ^* , which normalizes the space density. ϕ^* effectively measures the space density of $\sim L^*$ galaxies, and for both red and blue $\sim L^*$ galaxies, it approximately doubled from $z \sim 1.1$ to $z \sim 0.3$. Separate plots are shown for red, blue, and all galaxies (red data points), assuming fixed alpha values of -0.5 , -1.2 , and -1.0 , respectively. Shown for comparison are the results from Drory et al. (2003), Arnouts et al. (2007), and Cirasuolo et al. (2010), with the latter two plots varying smoothly because they are best fits to an evolving functional form. LFs for the low redshift universe are shown for Cole et al. (2001), Kochanek et al. (2001), Bell et al. (2003), Jones et al. (2006), Devereux et al. (2009), and Bonne et al. (2015) and labeled using square brackets. Error bars on our results show errors due to cosmic variance. Error bars on results from the literature are as published.

luminous red galaxy numbers via cessation of star formation. The evolution of the bright end of the red galaxy LF thus approximates the luminosity evolution of the most luminous red galaxies. Figure 17 shows how we used a Schechter function with variable α fitted to the bright end of the LF to measure the evolution of the bright end of the red galaxy LF at a space density of $\tilde{\phi} = 10^{-4.0} h_{70}^3 \text{ Mpc}^{-3} \text{ mag}^{-1}$.

Figure 18 plots the evolving absolute magnitude of galaxies having a space density of $\tilde{\phi} = 10^{-4.0} h_{70}^3 \text{ Mpc}^{-3} \text{ mag}^{-1}$, which measures the luminosity evolution of the most luminous galaxies. For red galaxies and blue galaxies, there are decreases

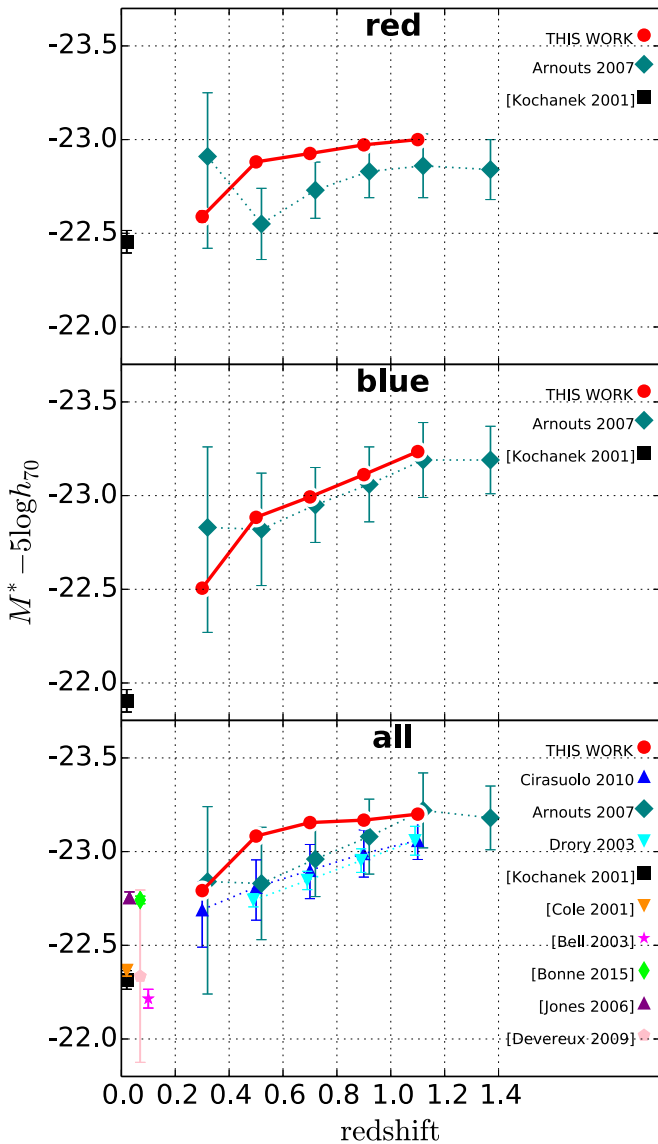


Figure 15. Evolution from $z = 1.1$ to $z = 0.3$ of the K -band maximum likelihood Schechter characteristic magnitude parameter $M_K^* - 5 \log h_{70}$. Separate plots are shown for red, blue, and all galaxies (red data points), assuming fixed alpha values of -0.5 , -1.2 , and -1.0 , respectively. M_K^* faded faster from $z = 1.1$ to $z = 0.3$ for blue galaxies ($\Delta M_K^* \sim 0.7$ mag) than for red ($\Delta M_K^* \sim 0.4$ mag). Also shown are results from the literature, as listed in each panel and referenced in the caption to Figure 14.

in luminosity of 0.19 mag and 0.33 mag (0.08 and 0.13 dex), respectively, from $z \sim 1.1$ to $z \sim 0.3$.

Figure 18 indicates that highly luminous red galaxies fade at an ever-increasing rate from $z \sim 1.1$ to $z \sim 0.3$. For a passively evolving model with a formation redshift of $z_f = 3.0$, we expect ~ 0.56 mag of fading in the K -band between $z = 1.1$ and $z = 0.3$. Given the ~ 0.1 mag fading we see in the absolute magnitudes of the brightest red galaxies, this implies that the most massive red galaxies increased in mass by a factor of ~ 1.4 between $z = 1.1$ and $z = 0.3$.

9.4. K -band Luminosity Evolution—Errors

Random and/or systematic uncertainties arise from the aperture photometry, photometric redshifts, cosmic variance, absolute magnitude determinations (K -corrections), Schechter

parameterization of the LF, choice of red/blue cut, and Eddington bias at the bright end. These uncertainties impact our measurements of evolution of the LF, the red galaxy luminosity density, and the luminosity of highly luminous red galaxies.

Because an important focus in this paper is to measure evolution of luminosity and stellar mass in red galaxies, we give order-of-magnitude estimates for uncertainties for red galaxies in Table 5. The table indicates how uncertainties propagate through our calculations of LF and red galaxy stellar mass evolution, and shows which uncertainties are of greatest significance. Note that all uncertainties in the table have been given in dex for consistency (e.g., magnitudes have been multiplied by 0.4). Most of the uncertainties are discussed in detail in Beare et al. (2014) and Beare et al. (2015), but we now discuss each of them in the context of the present paper.

Photometry. We discuss photometry first, as it forms the observational basis of all our work, enabling us to determine both galaxy luminosities and the photometric redshifts we used for the majority of galaxies. As described in Beare et al. (2015), our apparent magnitudes were measured using variable size photometric apertures and corrections for total flux. These aperture sizes and corrections were based on the analysis of growth curves of measured magnitude with aperture diameter for isolated galaxy images (i.e., those that did not overlap other objects). This method has the advantage that it is empirically based and does not assume any specific light profile (e.g., Sérsic, de Vaucouleurs, Petrosian, SDSS modelmag). Further, as described in Brown et al. (2007), the use of SExtractor segmentation maps largely eliminates flux from neighboring objects and corrects for the excluded flux.

We do not consider $(1+z)^{-4}$ cosmological surface brightness dimming (e.g., Calvi et al. 2014) to be a significant issue as the angular size at $z \sim 1$ of a large galaxy with half-light radius of 10 kpc is only 0.6 arcsec, and this is less than the FWHM of our 1.35 arcsec point-spread function. Such a galaxy would only be partially resolved and be approximately a point source, which largely mitigates the effect of cosmological surface brightness dimming.

Random uncertainties in measured apparent magnitudes arise from the aperture photometry and from the total flux corrections we make. Aperture photometry uncertainties are greater in some wavebands than others. Overall, averaged over all the galaxies with different apparent magnitudes in our sample, 1σ uncertainties are ~ 0.1 mag for B_W , R , I , and $[3.6 \mu\text{m}]$, ~ 0.2 mag for J and $[4.5 \mu\text{m}]$, ~ 0.4 mag for K . Uncertainties are significantly less for galaxies with brighter apparent magnitudes, as used in measuring the bright end of the K -band LF (and the massive end of the SMF). For example, 1σ K -band uncertainties for galaxies with reliable photometry in different redshift bins (the filled circles in Figures 7 to 9 are ~ 0.3 mag, but for galaxies with $M_K < -23$, as used in measuring evolution of the bright end of the LF, K -band uncertainties increase from 0.04 mag at $z \sim 0.3$ to 0.15 mag at $z \sim 1.1$). From our growth curves of magnitude with aperture diameter, we estimate that random uncertainties in the total flux corrections range from ~ 0.04 mag for the brightest objects to ~ 0.1 mag for the faintest. Adding these in quadrature to the uncertainties in aperture photometry, we obtain total random photometry errors ranging from ~ 0.1 mag to ~ 0.54 mag (~ 0.04 dex to ~ 0.22 dex in Table 5).

Table 4
K-band Luminosity Function Schechter Parameters for Fixed α

z	α	ϕ^* ($h_0^3 \text{Mpc}^{-3} \text{mag}^{-1}$)	$M_K^* - 5 \log h_{70}$	M_K at Fixed Space Density ^a (Measures Evolution of Most Luminous Galaxies)	j_K $L_\odot \text{Mpc}^{-3}$
Red galaxies - $\alpha = -0.5$					
0.3	-0.5	$3.14 \pm 0.10 \times 10^{-3}$	-22.59 ± 0.04	-24.13 ± 0.03	$3.50 \pm 0.24 \times 10^8$
0.5	-0.5	$2.29 \pm 0.10 \times 10^{-3}$	-22.88 ± 0.08	-24.24 ± 0.06	$3.33 \pm 0.31 \times 10^8$
0.7	-0.5	$2.25 \pm 0.10 \times 10^{-3}$	-22.93 ± 0.05	-24.31 ± 0.03	$3.43 \pm 0.15 \times 10^8$
0.9	-0.5	$2.01 \pm 0.20 \times 10^{-3}$	-22.97 ± 0.05	-24.35 ± 0.04	$3.19 \pm 0.44 \times 10^8$
1.1	-0.5	$1.75 \pm 0.13 \times 10^{-3}$	-23.00 ± 0.05	-24.32 ± 0.03	$2.85 \pm 0.24 \times 10^8$
Blue galaxies - $\alpha = -1.2$					
0.3	-1.2	$2.35 \pm 0.06 \times 10^{-3}$	-22.51 ± 0.05	-23.68 ± 0.05	$3.19 \pm 0.46 \times 10^8$
0.5	-1.2	$1.52 \pm 0.16 \times 10^{-3}$	-22.88 ± 0.09	-23.85 ± 0.08	$2.92 \pm 1.42 \times 10^8$
0.7	-1.2	$1.54 \pm 0.02 \times 10^{-3}$	-22.99 ± 0.05	-23.96 ± 0.06	$3.28 \pm 0.77 \times 10^8$
0.9	-1.2	$1.43 \pm 0.11 \times 10^{-3}$	-23.11 ± 0.06	-24.06 ± 0.04	$3.39 \pm 0.46 \times 10^8$
1.1	-1.2	$0.99 \pm 0.14 \times 10^{-3}$	-23.24 ± 0.09	-24.01 ± 0.07	$2.62 \pm 0.55 \times 10^8$
All galaxies - $\alpha = -1.0$					
0.3	-1.0	$4.34 \pm 0.25 \times 10^{-3}$	-22.79 ± 0.06	-24.19 ± 0.04	$6.58 \pm 0.90 \times 10^8$
0.5	-1.0	$3.15 \pm 0.23 \times 10^{-3}$	-23.08 ± 0.08	-24.31 ± 0.07	$6.25 \pm 1.51 \times 10^8$
0.7	-1.0	$3.14 \pm 0.09 \times 10^{-3}$	-23.16 ± 0.04	-24.40 ± 0.04	$6.64 \pm 0.66 \times 10^8$
1.1	-1.0	$3.11 \pm 0.22 \times 10^{-3}$	-23.17 ± 0.05	-24.47 ± 0.04	$6.67 \pm 0.83 \times 10^8$
1.1	-1.0	$2.67 \pm 0.19 \times 10^{-3}$	-23.20 ± 0.06	-24.46 ± 0.05	$5.89 \pm 0.76 \times 10^8$

Note.

^a $10^{-4.0} h_0^3 \text{Mpc}^{-3} \text{mag}^{-1}$ (M_K at this fixed space density is measured by fitting a Schechter function with variable α to the bright end of the LF).

Systematic uncertainties in aperture photometry will vary between different observing campaigns, and we do not attempt to estimate them here. However, we note that their major effect will be to shift computed luminosities by a constant factor without affecting evolutionary rates of change. We take systematic magnitude uncertainty due to our total flux corrections to be zero, as these corrections are as likely to be overestimates as underestimates.

Poisson uncertainties and cosmic variance. Poisson uncertainties in both the binned and the maximum likelihood space densities are greater at the bright end of the LF where galaxy numbers are fewer, as can be seen in Figures 7 to 13. Cosmic variance produces additional random uncertainty in space densities, which Beare et al. (2015) found using subfields to be $\sim 3\%$ for all galaxies (0.01 dex), and somewhat more for red galaxies that are more strongly clustered (i.e., $\sim 8\%$ [0.03 dex]). In combination, these two random uncertainties dominate in all redshift bins over systematic uncertainties arising from our very small systematic fractional photometric redshift errors, which are 0.02 at most. This size of systematic error changes the number of galaxies in a redshift bin of width 0.2 by less than 0.01 dex (e.g., at $z \sim 1$, a shift of 0.02 in the upper boundary of the bin, changes the number in the bin by a factor of $\sim 0.202/0.200$, and this equates to 0.0043 dex).

Luminosity errors. Errors in U -, B -, V -, and K -band luminosity measurements arise from photometric redshift uncertainties, photometry uncertainties, and uncertainties in K -correction calculations (Equation (1)). All these uncertainties are discussed in detail in Beare et al. (2014). Table 5 indicates how the three sources of uncertainty combine in the case of red galaxy luminosity calculations. K -correction uncertainties are due to the scatter of individual galaxies about the polynomials used to measure absolute magnitudes (Equation (1)). In Figure 2, the 1σ K -correction uncertainty is given in the top left-hand corner of the plot.

Photometric redshifts. Photometric redshift uncertainties impact our calculations in several ways: calculation of galaxy

luminosities (K -corrections), random and systematic uncertainties in binned and maximum likelihood LF numbers, Eddington bias at the bright end of the LF, and scattering of galaxies from one redshift bin to another.

As Figure 1 shows, our 1σ random fractional photometric redshift errors ($\lambda = [z_{\text{phot}} - z_{\text{spec}}]/[1 + z_{\text{phot}}]$) are ~ 0.05 (0.02 dex) or less. Our systematic fractional z_{phot} errors are very small, being < 0.01 (0.004 dex) for $0.2 < z_{\text{phot}} < 1.0$ and < 0.02 (0.008 dex) for $1.0 < z_{\text{phot}} < 1.2$.

The impact of photometric redshift errors is mitigated, especially at the bright end of the LF, by the use of spectroscopic redshifts, which are available for $\sim 75\%$ of red and blue $I < 19.5$ galaxies and $\sim 45\%$ of $I < 20.5$ galaxies.

Photometric redshift uncertainties perturb measured K -band reframe magnitudes by altering distance moduli D_M in Equation (1). Assuming an approximate inverse square law, the fractional uncertainties in measured luminosities will be twice the fractional uncertainties in z_{phot} values (i.e., random fractional uncertainties of ~ 0.02 dex, and systematic fractional uncertainties of 0.01 dex for $0.2 < z_{\text{phot}} < 1.0$ and ~ 0.02 dex for $1.0 < z_{\text{phot}} < 1.2$).

It is important to realize that these estimated errors arising from z_{phot} errors are for individual galaxies. In the case of systematic redshift errors, the impact on *evolutionary* measurements depends on the distribution of z_{phot} errors with redshift. Figure 1 shows that photometric redshifts are very slightly overestimated at $z \sim 0.25$ and $z \sim 0.7$, and underestimated at $z \sim 1.0$. We do not pursue this further here, beyond noting that the effect of z_{phot} errors on evolutionary measurements will potentially be comparable with that on individual values.

To gauge the impact of systematic z_{phot} errors, we repeated all our calculations twice using z_{phot} values increased and decreased by the fractional systematic error over most of the redshift range (i.e., $0.2 < z \leq 1.0$), as shown in Figure 1. This was $\lambda = [z_{\text{phot}} - z_{\text{spec}}]/[1 + z_{\text{phot}}] = 0.01$. For the increased (decreased) z_{phot} values, red galaxy luminosity density values decreased (increased) by up to ~ 0.02 dex, while massive red

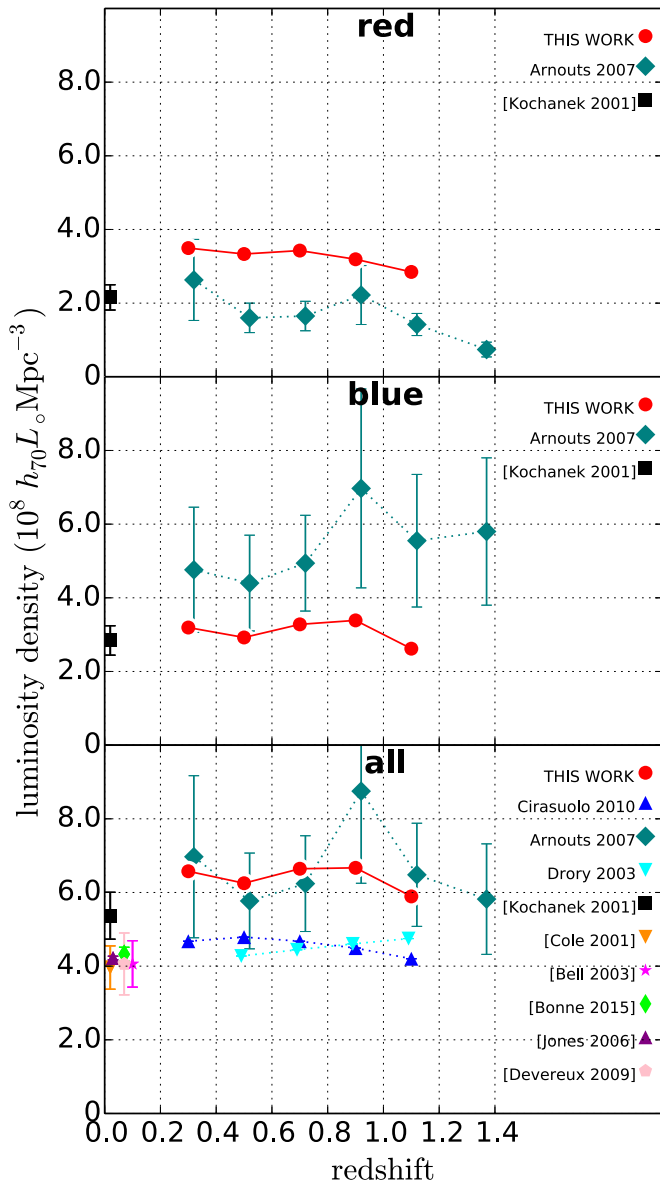


Figure 16. K -band luminosity density of both red and blue galaxies increased by a modest factor of ~ 1.2 from $z = 1.1$ to $z = 0.3$. Separate plots are shown for red, blue, and all galaxies (red data points), assuming fixed α values of -0.5 , -1.2 , and -1.0 , respectively. Also shown are results from the literature, as listed in each panel and referenced in the caption to Figure 14. Red galaxy SMD grows at steady rate, and for red galaxies the increase in luminosity density with decreasing redshift implies a buildup of stellar mass, because passively evolving stellar populations fade as they evolve.

galaxies showed a luminosity increase (decrease) of up to ~ 0.01 dex.

To measure the effect of the random z_{phot} uncertainties $\lambda = [z_{\text{phot}} - z_{\text{spec}}]/[1 + z_{\text{phot}}] = 0.05$, we repeated our calculations 10 times, each time applying normally distributed random fractional errors ($\sigma = 0.05$) to individual z_{phot} values. Our results are shown in the penultimate section of Table 5. We found that individual measured values of both red galaxy luminosity density and highly luminous red galaxy luminosity differed between simulations by less than 0.01 dex, indicating that random photometric redshift errors did not produce significant scatter in these two measurements.

However, due to random z_{phot} uncertainties, the measured luminosities of luminous red galaxies (at fixed space density)

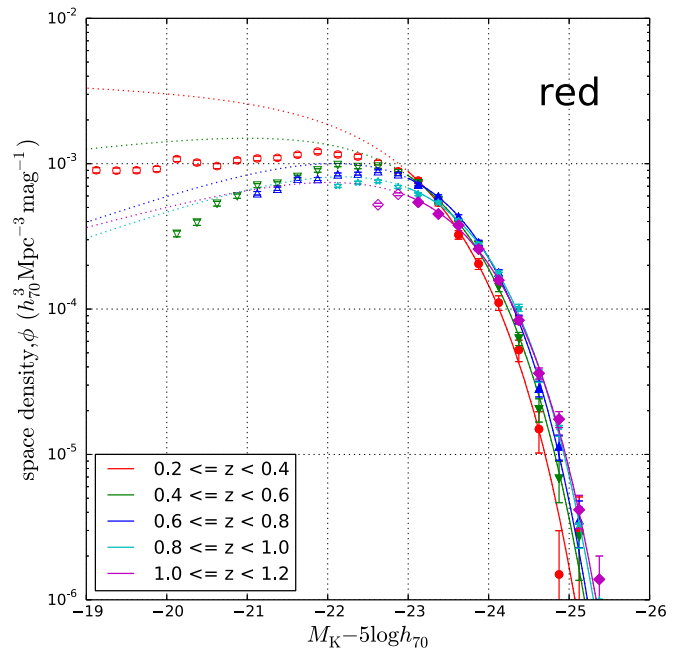


Figure 17. How evolution of the K -band highly luminous red galaxies was measured by fitting a Schechter function with variable α parameter to just the brightest part of the LF. Symbols are as in Figure 11.

showed a small systematic shift which increased from ~ 0.01 dex for $0.2 < z \leq 0.4$ to ~ 0.04 for $1.0 < z \leq 1.2$. This shift is partly an Eddington shift (Eddington 1913) caused by greater numbers of galaxies being randomly scattered to higher luminosities than to lower luminosities, on account of the steeply declining exponential shape of the LF at high luminosity. The remainder of the observed systematic shift is due to galaxies being scattered between redshift bins: if the LF evolves with redshift, this scattering across redshift bin boundaries will modify the measured LFs in individual redshift bins. As the fraction of red galaxies with spectroscopic redshifts decreases with increasing redshift, the impact of redshift errors on the bright end of the LF increases with redshift. All these different effects of random redshift errors are highly correlated and very difficult to analyze analytically. This is the reason why we used Monte Carlo simulations to measure the overall effect of random z_{phot} uncertainties.

Monte Carlo simulations also show that random z_{phot} errors give rise to a systematic decrease in measured luminosity density. This systematic error ranges from ~ 0.01 dex at $0.2 < z \leq 0.4$, where a significant proportion of galaxies have accurate spectroscopic redshifts, to 0.07 dex at $1.0 < z \leq 1.2$, where few galaxies have spectroscopic redshifts. The error in measured luminosity densities can be attributed to galaxies being scattered across redshift bin boundaries with changed measured luminosities. For example, a galaxy with $\Delta z_{\text{phot}} = 0.05$ and $z = 0.98$ will be scattered upward across the $z = 1$ boundary into the next redshift bin, and its measured luminosity will be increased by $\sim 10\%$, assuming an approximate inverse square law. The space density at the faint end of the LF increases with increasing luminosity, rather than decreases, so at this end there is a net flow of galaxies to lower redshift bins and lower luminosities. The observed systematic change in luminosity density in each redshift bin is the net result of perturbed luminosity values and of galaxies

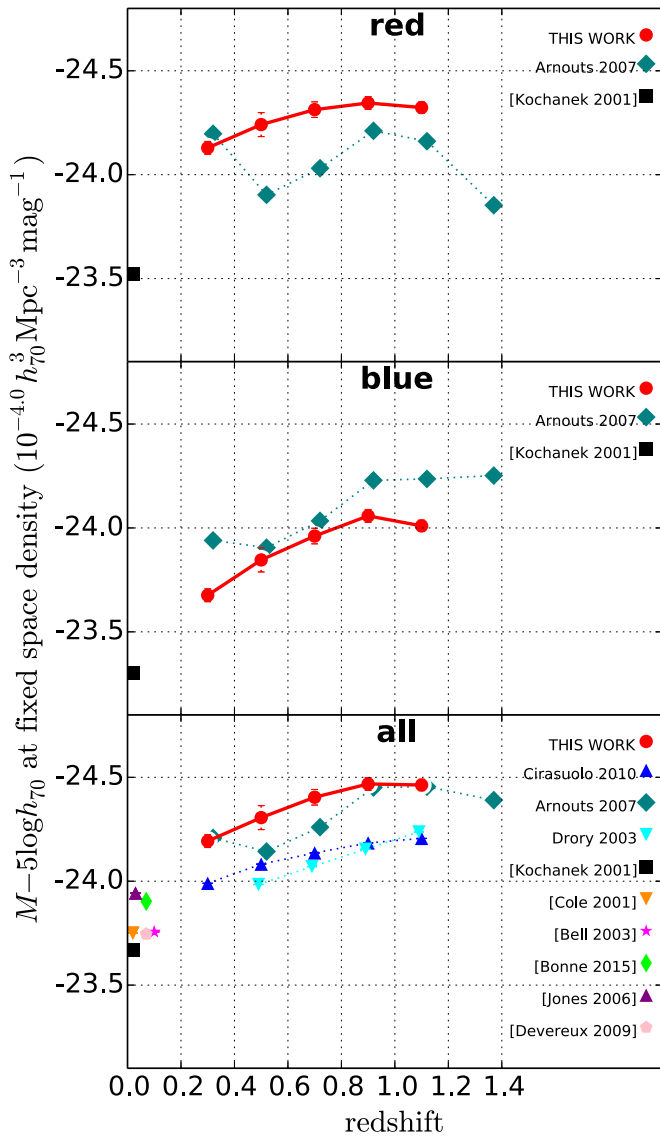


Figure 18. Evolution of the bright end of the K -band LF. The luminosity of the brightest blue galaxies decreases by ~ 0.33 mag from $z = 1.1$ to $z = 0.3$. For red galaxies, the smaller decrease of ~ 0.19 mag represents the fading of individual highly luminous red galaxies offset by additional luminosity gained through minor mergers. The rate of fading increases with time. The value $\bar{M}_K - 5 \log h_{70}$ corresponding to a space density of $10^{-4.0} h_{70}^3 \text{ Mpc}^{-3} \text{ mag}^{-1}$ is used to measure evolution of the luminosity of the brightest galaxies from $z \sim 1.1$ to $z \sim 0.3$. The separate plots shown for red, blue, and all galaxies (red data points) assume fixed α values of -0.5 , -1.2 , and -1.0 , respectively. Also shown are results from the literature, as listed in each panel and referenced in the caption to Figure 14.

being scattered in and out of the redshift bin at the upper and lower bin boundaries.

In addition to random photometric redshift errors, random photometry and K -correction errors also contribute to the random errors in our K -band luminosity measurements. This increases the Eddington shift in our measurements of the bright end of the LF for red galaxies. We modeled the photometric and K -correction errors by convolving the Schechter function for red galaxies with a Gaussian with $\sigma = 0.03$ dex (Table 5) and found that the resultant shift in the luminosity corresponding to our fixed space density of $\bar{\phi} = 10^{-4.0} h_{70}^3 \text{ Mpc}^{-3} \text{ mag}^{-1}$ was increased by 0.03 dex.

Schechter parameterization. In measuring the evolution of the K -band LF and the K -band luminosity density, uncertainty arises from parameterizing the LF using a single Schechter function and using this parameterization to compute these quantities. Beare et al. (2015) found that the B -band luminosity density varied by less than 0.03 dex when α was varied by ± 0.1 , pointing out that for red galaxies, it is insensitive to the exact value of α chosen, even though M^* and ϕ^* vary considerably. We assume that similar conclusions will apply in the case of the K -band LF, and take 0.03 dex as the random uncertainty in K -band luminosity density due to the inexactness of the Schechter parameterization.

Red-blue cut. Our evolving red-blue cut is intended to separate quiescent and star-forming galaxies, but the correspondence is not exact, due to factors such as residual star formation in some quiescent galaxies, and dust obscuration, which causes some star-forming galaxies to appear redder than they really are. The best position to adopt for the red-blue cut involves some uncertainty. We investigated this in Beare et al. (2015) and found that moving the position of the cut up or down by 0.05 mag made 0.05 dex difference to the measured optical luminosity density of red galaxies and 0.02 dex difference to the measured luminosity of luminous red galaxies. We assume here that similar differences will apply to the K -band LF and the SMF.

* *Conclusion.* Table 5 shows that systematic errors in red galaxy luminosity density range from ~ 0.06 dex at $z = 0.3$ to ~ 0.12 dex at $z = 1.1$, and are larger than the random uncertainties of ~ 0.04 dex. Potentially, correcting for the change in systematic error with redshift could decrease the measured increase of luminosity density from $z = 1.1$ to $z = 0.3$ by ~ 0.06 dex, altering the luminosity density growth from 0.08 ± 0.04 dex ($\times 1.20 \pm 0.11$) to 0.02 ± 0.04 dex ($\times 1.05 \pm 0.10$).

Systematic errors in the measured luminosity of highly luminous red galaxies range from ~ 0.08 dex at $z = 0.3$ to ~ 0.13 dex at $z = 1.1$ and dominate the random uncertainties, which Monte Carlo simulations show to be less than 0.01 dex. Potentially, correcting for the change in systematic error with redshift could decrease the measured luminosity fading of highly luminous red galaxies from $z = 1.1$ to $z = 0.3$ by ~ 0.05 dex, altering the measured luminosity decrease from 0.08 ± 0.01 dex ($\times 0.83 \pm 0.03$) to 0.03 ± 0.01 dex ($\times 0.93 \pm 0.02$).

To summarize, systematic errors could significantly reduce the 20% growth in red galaxy luminosity density to 5% and significantly reduce the 17% fading of luminous red galaxies to 7%.

9.5. K -band Luminosity Evolution—Comparison with the Literature

As Figures 7 and 10 show, the bright end of our LF for all galaxies at $0.2 \leq z < 0.4$ is ~ 0.3 mag brighter than the LFs reported by several authors for the low redshift ($z < 0.2$) universe.

A small part of this difference will be due to evolution of the LF between $z \sim 0.3$ and $z \sim 0.1$, but we expect our measured magnitudes to be brighter than those from studies such as Cole et al. (2001), Kochanek et al. (2001), Bell et al. (2003), and Bonne et al. (2015), which used the Two Micron All Sky Survey extended source catalog data (2MASS, Jarrett et al. 2000). Because 2MASS is relatively shallow, the faint outer parts of extended sources become lost in the 2MASS sky

Table 5
Order-of-magnitude Estimates of Random and Systematic Errors for Red Galaxies—in Dex

Quantity	Details of Error	Random	Systematic
OBSERVATIONAL ERRORS			
Photometry errors	Aperture photometry errors (0.02 to 0.4 mag)	0.01 to 0.16 ^a	0.01
	Total flux correction from growth curves (0.1 to 0.2 mag)	0.04 to 0.1	0.01
	$(1+z)^{-4}$ cosmological surface brightness dimming	<0.01	<0.01
	TOTAL	0.04 to 0.19	0.02
Photometric redshift errors	$\lambda = (z_p - z_s)/(1 + z_s) = 0.05$ (random), 0.02 (systematic)	0.02	0.01
Space density uncertainties	Cosmic variance uncertainty—8% by subfields	0.03	...
ERRORS IN DERIVED QUANTITIES FOR INDIVIDUAL GALAXIES			
Luminosity errors (U, B, V, K) (in dex, not mag)	Due to photometric redshift errors	0.04	0.02
	Due to photometry errors (as noted previously)	0.02–0.19 ^a	0.02
	Due to K-correction errors (Equation (1))	0.02	0.01
	TOTAL	0.05 to 0.20 ^a	0.05
M/L_K errors	Inaccuracy of M/L_K formula (Equations (3) and (5))	0.10	0.03
	Dependence of M/L_K formula on assumed SPS model, SFH, metallicity, and dust	...	0.30
	(may not significantly affect relative mass growth)	...	[0.30]
	Dependence of M/L_K formula on assumed IMF (does not affect relative mass growth)	...	[0.30]
	Impact of photometric redshift errors on evolving M/L_K formula (Equations(3) and (5))	0.02	0.01
	TOTAL (ignoring SPS and IMF error)	0.10	0.04
	Stellar mass errors	Due to M/L_K error (as noted previously)	0.10
	Due to K -band luminosity error (as noted previously)	0.05 to 0.20 ^a	0.05
	TOTAL	0.11 to 0.22 ^a	0.09
UNCERTAINTIES IN EVOLVING RED GALAXY LUMINOSITY DENSITIES AND STELLAR MASS DENSITIES			
Evolving K -band luminosity density errors for red galaxies	Due to K -band luminosity errors (as above)	...	0.05
	Due to cosmic variance	0.03	...
	Due to inexactness of the Schechter parameterization	0.03	...
	Error due to z_{phot} scattering across redshift bin boundaries ^b	...	0.01–0.07 ^c
	TOTAL	0.04	0.06–0.12
Evolving SMD errors for red galaxies	Due to stellar mass errors (as noted previously)	...	0.09 ^d
	Due to cosmic variance	0.03	...
	Due to inexactness of the Schechter parameterization	0.03	...
	Error due to z_{phot} scattering across redshift bin boundaries ^b	...	0.01 – 0.09 ^c
	TOTAL	0.04	0.10–0.18 ^d
UNCERTAINTIES IN EVOLVING K-BAND LUMINOSITIES AND STELLAR MASSES OF LUMINOUS/MASSIVE RED GALAXIES			
K -band luminosity errors for highly luminous red galaxies	Due to K -band luminosity errors	<0.01	0.05
	Eddington bias from $\sigma = 0.03$ scatter in K -band luminosities due to photometry and K-corrections (but not z_{phot} errors)	...	0.03
	Eddington bias due to random z_{phot} errors and bias due to z_{phot} scattering across redshift bin boundaries ^b	<0.01	0.001 – 0.04 ^c
	TOTAL	0.01	0.08 – 0.13 ^c
	Stellar mass errors for massive red galaxies	Due to stellar mass errors	<0.01
	Eddington bias from $\sigma = 0.1$ scatter in $\log_{10}(M/L_K)$ (Equation (5))	...	0.22
	Eddington bias due to random z_{phot} errors and bias due to z_{phot} scattering across redshift bin boundaries ^b	<0.01	0.001 – 0.04 ^c
	TOTAL	0.01	0.11–0.15 ^c
NET EFFECT ON RED GALAXY RESULTS OF RANDOM FRACTIONAL PHOTOMETRIC REDSHIFT ERROR $\sigma = 0.05$ (FROM SIMULATION)			
Red galaxy K -band luminosity density		≤ 0.01	0.01–0.07 ^c
K -band luminosity at fixed space density for luminous red galaxies		≤ 0.01	0.001–0.04 ^c
Red galaxy stellar mass density		≤ 0.01	0.01–0.09 ^c
Stellar mass \tilde{M} at fixed space density for massive red galaxies		≤ 0.01	0.001–0.04 ^c
NET EFFECT ON RED GALAXY RESULTS OF SYSTEMATIC FRACTIONAL PHOTOMETRIC REDSHIFT ERROR OF +0.01 (FROM SIMULATION)			
Red galaxy K -band luminosity density		...	–0.02
		...	–0.01

Table 5
(Continued)

Quantity	Details of Error	Random	Systematic
<i>K</i> -band luminosity at fixed space density for luminous red galaxies			
Red galaxy stellar mass density		...	−0.03
Stellar mass \bar{M} at fixed space density for massive red galaxies		...	−0.01

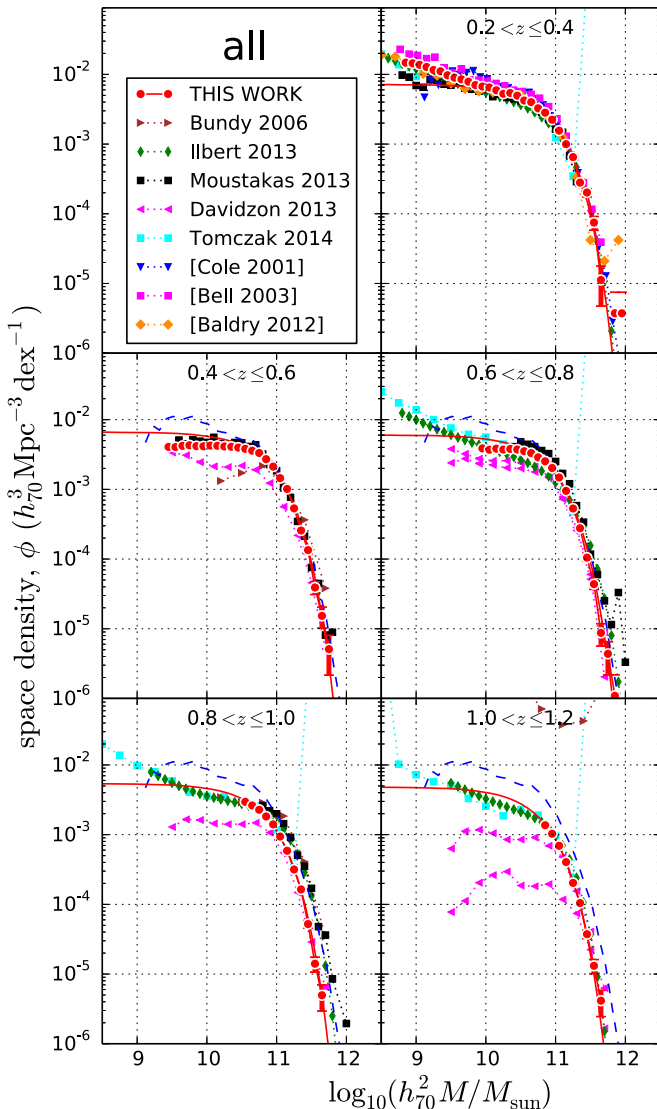
Notes.^a Aperture photometry errors depend on the waveband and increase with apparent magnitude.^b From Monte Carlo simulations, as shown later.^c Error increases with redshift, largely due to decreasing proportion of accurate spectroscopic redshifts.^d Assuming no uncertainty due to variation with redshift of SPS model predictions of stellar mass.

Figure 19. Binned SMFs for all galaxies based on *K*-band *M/L* ratios with $1 - \sigma$ Poisson uncertainties shown for the Boötes data. Overplotted in red are maximum likelihood fits to the (unbinned) data. We show the evolving SMFs from Bundy et al. (2006), Davidzon et al. (2013), Ilbert et al. (2013), Moustakas et al. (2013), and Tomczak et al. (2014) for comparison, as well as SMFs for the low redshift universe from Cole et al. (2001), Bell et al. (2003), and Baldry et al. (2012). The Cole et al. (2001) SMF for all galaxies in the low redshift universe is shown in the lower four plots as a black dashed line in order to provide a fixed reference. The plots from Davidzon et al. (2013) are for $z \sim 0.55, 0.65, 0.75, 0.85, 1.0,$ and 1.2 .

background. Andreon (2002) demonstrated that the isophotal magnitude models used by authors such as Kochanek et al. (2001) and Cole et al. (2001) underestimate the flux from extended sources by even more than the ~ 0.2 mag that these authors predicted, even in the case of bright galaxies. Andreon (2002) also showed that 2MASS failed to detect low surface brightness galaxies.

By contrast, we accounted for light falling outside the photometric aperture by using growth curves of measured apparent magnitude with aperture size (Beare et al. 2015). For example, for a galaxy with an apparent *I*-band magnitude of 20.5 mag, we used an aperture of diameter 8 arcsec and made a correction for missing flux of -0.070 mag, while at magnitude -23.5 we used a 3 arcsec aperture and made a correction of -0.302 . In Beare et al. (2015), we compared our photometry with MAG_AUTO and found it to be brighter by ~ 0.06 mag for $I < 20$, rising to ~ 0.13 at $I = 24$. These factors adequately account for the difference between our LFs and those based on 2MASS, as seen in Figures 7 to 10.

Local surveys do have a strong dependence on the type of photometry used, but an advantage of a deep survey like ours with partially resolved galaxies is a reduced dependence on the intrinsic light profiles of the galaxies. For example, when the galaxy is far smaller than the PSF, aperture photometry with PSF corrections is adequate. A deep survey, with high signal-to-noise, can also afford to use oversized apertures for photometry of large galaxies, whereas shallower surveys using comparable apertures could be swamped by noise.

Figure 7 shows that at higher redshifts, agreement with the evolving LFs for all galaxies of Drory et al. (2003) and Cirasuolo et al. (2010) is somewhat uneven: it is closer at some redshifts than others. Both these studies used photometric redshifts, as we did, but their sample sizes were much smaller than ours (~ 70 and ~ 10 times smaller, respectively), so larger Poisson errors and cosmic variance can explain why there were greater differences from our work at some redshifts versus others.

Figures 14 and 15 compare our measurements of the evolution of ϕ_K^* and M_K^* with those of Cirasuolo et al. (2010), Arnouts et al. (2007), and Drory et al. (2003), and show values for the low redshift universe from several authors. Cirasuolo et al. (2010) and Arnouts et al. (2007) fitted an evolving functional form to their data so that their parameters were forced to vary smoothly with redshift.

It is difficult to compare ϕ_K^* and M_K^* evolution measurements from different studies because the well-known degeneracy between the Schechter parameters means that different α value choices give rise to different measured values for ϕ^* and

Table 6
Stellar Mass Function Schechter Parameters Based on K , V and i -band Mass-to-light Ratios

z	α	ϕ^* ($h_7^3 \text{Mpc}^{-3} \log_{10} M^{-1}$)	$\log_{10} M^*/M_\odot$	$\log_{10} M/M_\odot$ at Fixed Space Density ^a (Measures Evolution of Most Massive Galaxies)	\log_{10} Stellar Mass Density ($h_7^3 M_\odot \text{Mpc}^{-3}$)
Red galaxies					
0.3	-0.5	$2.90 \pm 0.11 \times 10^{-3}$	10.78 ± 0.07	11.47 ± 0.07	8.19 ± 0.02
0.5	-0.5	$2.35 \pm 0.16 \times 10^{-3}$	10.79 ± 0.04	11.42 ± 0.08	8.11 ± 0.03
0.7	-0.5	$2.27 \pm 0.11 \times 10^{-3}$	10.78 ± 0.04	11.40 ± 0.06	8.08 ± 0.02
0.9	-0.5	$1.88 \pm 0.04 \times 10^{-3}$	10.73 ± 0.06	11.31 ± 0.05	7.95 ± 0.01
1.1	-0.5	$1.46 \pm 0.13 \times 10^{-3}$	10.71 ± 0.05	11.24 ± 0.10	7.82 ± 0.04
Blue galaxies					
0.3	-1.2	$1.78 \pm 0.04 \times 10^{-3}$	10.59 ± 0.06	11.10 ± 0.05	7.90 ± 0.01
0.5	-1.2	$0.99 \pm 0.04 \times 10^{-3}$	10.79 ± 0.04	11.17 ± 0.03	7.85 ± 0.02
0.7	-1.2	$0.97 \pm 0.02 \times 10^{-3}$	10.79 ± 0.04	11.16 ± 0.03	7.85 ± 0.01
0.9	-1.2	$1.04 \pm 0.04 \times 10^{-3}$	10.67 ± 0.05	11.04 ± 0.04	7.75 ± 0.02
1.1	-1.2	$0.74 \pm 0.05 \times 10^{-3}$	10.66 ± 0.08	10.95 ± 0.06	7.59 ± 0.03
All galaxies					
0.3	-1	$3.13 \pm 0.06 \times 10^{-3}$	10.87 ± 0.08	11.48 ± 0.07	8.36 ± 0.01
0.5	-1	$2.90 \pm 0.13 \times 10^{-3}$	10.86 ± 0.03	11.43 ± 0.05	8.32 ± 0.02
0.7	-1	$2.62 \pm 0.06 \times 10^{-3}$	10.88 ± 0.03	11.42 ± 0.04	8.29 ± 0.01
0.9	-1	$2.36 \pm 0.08 \times 10^{-3}$	10.80 ± 0.05	11.33 ± 0.04	8.17 ± 0.01
1.1	-1	$2.09 \pm 0.16 \times 10^{-3}$	10.76 ± 0.05	11.27 ± 0.05	8.08 ± 0.03

Note.

^a $2.5 \times 10^{-4.0} h_7^3 \text{Mpc}^{-3} \text{dex}^{-1}$. ($\log_{10} M/M_\odot$ at this fixed space density is measured by fitting a Schechter function with variable α to the massive end of the SMF.)

Table 7
Binned K -band Luminosity Function for All Galaxies

$M_K - 5 \log h_7$		Luminosity Function ($10^{-3} h_7^3 \text{Mpc}^{-3} \text{mag}^{-1}$)				
Min	Max	$0.2 \leq z < 0.4$	$0.4 \leq z < 0.6$	$0.6 \leq z < 0.8$	$0.8 \leq z < 1.0$	$1.0 \leq z < 1.2$
-26.00	-25.75	...	0.001 ± 0.001
-25.75	-25.50	0.001 ± 0.001
-25.50	-25.25	0.001 ± 0.001	0.001 ± 0.001
-25.25	-25.00	0.003 ± 0.002	0.003 ± 0.001	0.004 ± 0.001	0.005 ± 0.001	0.008 ± 0.001
-25.00	-24.75	0.001 ± 0.001	0.007 ± 0.002	0.015 ± 0.003	0.022 ± 0.003	0.026 ± 0.003
-24.75	-24.50	0.018 ± 0.005	0.027 ± 0.004	0.037 ± 0.004	0.055 ± 0.004	0.052 ± 0.004
-24.50	-24.25	0.060 ± 0.009	0.072 ± 0.007	0.113 ± 0.007	0.137 ± 0.007	0.125 ± 0.006
-24.25	-24.00	0.134 ± 0.014	0.176 ± 0.011	0.241 ± 0.010	0.254 ± 0.009	0.241 ± 0.008
-24.00	-23.75	0.248 ± 0.019	0.365 ± 0.016	0.420 ± 0.014	0.436 ± 0.012	0.396 ± 0.011
-23.75	-23.50	0.453 ± 0.026	0.561 ± 0.020	0.646 ± 0.017	0.657 ± 0.015	0.573 ± 0.013
-23.50	-23.25	0.759 ± 0.034	0.860 ± 0.024	0.919 ± 0.020	0.894 ± 0.017	0.729 ± 0.015
-23.25	-23.00	1.122 ± 0.041	1.137 ± 0.028	1.183 ± 0.023	1.101 ± 0.019	0.924 ± 0.017
-23.00	-22.75	1.369 ± 0.045	1.428 ± 0.031	1.458 ± 0.025	1.293 ± 0.021	1.085 ± 0.018
-22.75	-22.50	1.617 ± 0.049	1.665 ± 0.034	1.645 ± 0.027	1.524 ± 0.023	1.149 ± 0.019
-22.50	-22.25	2.017 ± 0.055	1.737 ± 0.034	1.775 ± 0.028	1.648 ± 0.024	...
-22.25	-22.00	2.255 ± 0.058	1.969 ± 0.037	1.892 ± 0.029	1.745 ± 0.025	...
-22.00	-21.75	2.602 ± 0.062	2.012 ± 0.037	1.960 ± 0.030	1.800 ± 0.025	...
-21.75	-21.50	2.738 ± 0.064	2.074 ± 0.038	2.152 ± 0.031	1.827 ± 0.025	...
-21.50	-21.25	2.957 ± 0.066	2.121 ± 0.038	2.150 ± 0.031
-21.25	-21.00	3.195 ± 0.069	2.176 ± 0.039	2.298 ± 0.033
-21.00	-20.75	3.437 ± 0.072	2.191 ± 0.039	2.226 ± 0.032
-20.75	-20.50	3.638 ± 0.074	2.153 ± 0.039
-20.50	-20.25	4.152 ± 0.079	2.053 ± 0.038
-20.25	-20.00	4.707 ± 0.084	2.001 ± 0.038
-20.00	-19.75	5.062 ± 0.087	1.917 ± 0.037
-19.75	-19.50	5.599 ± 0.092
-19.50	-19.25	6.164 ± 0.097
-19.25	-19.00	6.661 ± 0.101
-19.00	-18.75	6.876 ± 0.103
-18.75	-18.50	7.338 ± 0.107
-18.50	-18.25	6.987 ± 0.105

Table 8
Binned K -band Luminosity Function for Red Galaxies

$M_K - 5 \log h_{70}$		Luminosity Function ($10^{-3} h_{70}^3 \text{ Mpc}^{-3} \text{ mag}^{-1}$)				
Min	Max	$0.2 \leq z < 0.4$	$0.4 \leq z < 0.6$	$0.6 \leq z < 0.8$	$0.8 \leq z < 1.0$	$1.0 \leq z < 1.2$
-26.00	-25.75	...	0.001 ± 0.001
-25.75	-25.50
-25.50	-25.25	0.001 ± 0.001	0.001 ± 0.001
-25.25	-25.00	0.003 ± 0.002	0.003 ± 0.001	0.004 ± 0.001	0.003 ± 0.001	0.004 ± 0.001
-25.00	-24.75	0.001 ± 0.001	0.007 ± 0.002	0.011 ± 0.002	0.016 ± 0.002	0.017 ± 0.002
-24.75	-24.50	0.015 ± 0.005	0.020 ± 0.004	0.028 ± 0.004	0.035 ± 0.003	0.036 ± 0.003
-24.50	-24.25	0.052 ± 0.009	0.063 ± 0.007	0.085 ± 0.006	0.102 ± 0.006	0.084 ± 0.005
-24.25	-24.00	0.111 ± 0.013	0.142 ± 0.010	0.178 ± 0.009	0.176 ± 0.008	0.158 ± 0.007
-24.00	-23.75	0.205 ± 0.017	0.276 ± 0.014	0.286 ± 0.011	0.276 ± 0.010	0.259 ± 0.009
-23.75	-23.50	0.324 ± 0.022	0.382 ± 0.016	0.432 ± 0.014	0.403 ± 0.012	0.377 ± 0.010
-23.50	-23.25	0.541 ± 0.028	0.558 ± 0.019	0.594 ± 0.016	0.540 ± 0.014	0.451 ± 0.012
-23.25	-23.00	0.764 ± 0.034	0.732 ± 0.022	0.717 ± 0.018	0.617 ± 0.015	0.543 ± 0.013
-23.00	-22.75	0.888 ± 0.036	0.859 ± 0.024	0.846 ± 0.019	0.694 ± 0.015	0.616 ± 0.014
-22.75	-22.50	1.013 ± 0.039	0.955 ± 0.025	0.888 ± 0.020	0.757 ± 0.016	0.522 ± 0.013
-22.50	-22.25	1.119 ± 0.041	0.948 ± 0.025	0.854 ± 0.019	0.742 ± 0.016	...
-22.25	-22.00	1.157 ± 0.042	0.979 ± 0.026	0.844 ± 0.019	0.704 ± 0.016	...
-22.00	-21.75	1.212 ± 0.043	0.898 ± 0.025	0.785 ± 0.019
-21.75	-21.50	1.152 ± 0.041	0.810 ± 0.024	0.786 ± 0.019
-21.50	-21.25	1.097 ± 0.040	0.728 ± 0.022	0.672 ± 0.018
-21.25	-21.00	1.087 ± 0.040	0.707 ± 0.022	0.626 ± 0.017
-21.00	-20.75	1.055 ± 0.040	0.598 ± 0.021
-20.75	-20.50	0.963 ± 0.038	0.530 ± 0.019
-20.50	-20.25	1.018 ± 0.039	0.393 ± 0.017
-20.25	-20.00	1.076 ± 0.040	0.329 ± 0.016
-20.00	-19.75	0.919 ± 0.037
-19.75	-19.50	0.901 ± 0.037
-19.50	-19.25	0.896 ± 0.037
-19.25	-19.00	0.901 ± 0.037
-19.00	-18.75	0.867 ± 0.037
-18.75	-18.50	0.808 ± 0.036
-18.50	-18.25	0.720 ± 0.034
-18.25	-18.00	0.630 ± 0.032

M_K^* —for example, for the B -band LF of all galaxies at $0.2 \leq z < 0.4$, Beare et al. (2015) found that increasing α from -1.1 to -1.0 decreased ϕ_B^* by $\sim 20\%$ while making $M_B^* \sim 0.1$ mag brighter. The value $\alpha = -0.9$ adopted by Cirasuolo et al. (2010) and Drory et al. (2003) for all galaxies is 0.1 greater than our value of -1.0 , and this explains their fainter M_K^* and smaller ϕ_K^* values. Similarly, at low redshift, discrepancies between different authors are accounted for by differences in the α values adopted, with Jones et al. (2006) and Bonne et al. (2015) using the largest (most negative) values (see values in Table 6 of Bonne et al. 2015).

Taking into account the degeneracy among ϕ_K^* , M_K^* , and α ; the lower faint-end space densities and fainter magnitudes expected from studies based on 2MASS; and the different subsample criteria used by different authors, we conclude that our ϕ_K^* and M_K^* measurements are not inconsistent with those from previous studies.

Figure 16 shows that we measured a higher luminosity density at all redshifts for all galaxies than the studies of Cirasuolo et al. (2010) and Drory et al. (2003), while obtaining comparable values to Arnouts et al. (2007), but much smoother evolution. Our measured luminosity density at low redshift is higher than the literature, much of which utilizes the relatively shallow 2MASS data.

As Figure 18 shows, bright end galaxies were 0.2 to 0.3 mag brighter than those in Cirasuolo et al. (2010) and Drory et al. (2003), and varied more smoothly in luminosity than those of

Arnouts et al. (2007). Recent studies (e.g., D’Souza et al. 2015; Loveday et al. 2015; Bernardi et al. 2016) have shown that measurements of the bright end of the LF are highly sensitive to the photometric model used (e.g., Sérsic, Petrosian, SDSS cmodel), as this affects how much light from the faint outer edges of extended galaxies is measured. Our photometric corrections based on growth curves were model independent and should have provided good estimates of total galaxy light, even though we did not derive different corrections for quiescent and star-forming galaxies, which generally exhibit de Vaucouleurs and Sérsic light profiles, respectively. We therefore expect the bright end of our LFs to be brighter than much of the literature, and Figures 7 to 9 show that this is the case by ~ 0.3 mag.

10. Stellar Mass Evolution—Results and Discussion

10.1. Evolution of the SMF

In order to compare our SMF results with the literature, we plot our binned SMFs alongside those from a variety of previous studies in Figures 19 to 22. Our binned SMFs are tabulated in Tables 10–12. Maximum likelihood fits to our (unbinned) data are overplotted as continuous red lines. To provide a fixed reference in the plots, we show the local SMF for all galaxies (i.e., red and blue combined) from Cole et al. (2001) in each bin. We only plot bins for which 97.7% (the 2σ limit) or more of the measured masses correspond to magnitudes brighter than our faint limit of $I = 24.0$.

Table 9
Binned K -band Luminosity Function for Blue Galaxies

$M_K - 5 \log h_{70}$		Luminosity Function ($10^{-3} h_{70}^3 \text{ Mpc}^{-3} \text{ mag}^{-1}$)				
Min	Max	$0.2 \leq z < 0.4$	$0.4 \leq z < 0.6$	$0.6 \leq z < 0.8$	$0.8 \leq z < 1.0$	$1.0 \leq z < 1.2$
-25.75	-25.50	0.001 ± 0.001
-25.50	-25.25
-25.25	-25.00	0.001 ± 0.001	0.001 ± 0.001	0.004 ± 0.001
-25.00	-24.75	...	0.001 ± 0.001	0.004 ± 0.001	0.007 ± 0.001	0.008 ± 0.001
-24.75	-24.50	0.003 ± 0.002	0.007 ± 0.002	0.008 ± 0.002	0.020 ± 0.003	0.016 ± 0.002
-24.50	-24.25	0.007 ± 0.003	0.010 ± 0.003	0.028 ± 0.003	0.035 ± 0.003	0.042 ± 0.003
-24.25	-24.00	0.024 ± 0.006	0.035 ± 0.005	0.063 ± 0.005	0.079 ± 0.005	0.083 ± 0.005
-24.00	-23.75	0.043 ± 0.008	0.088 ± 0.008	0.134 ± 0.008	0.161 ± 0.007	0.137 ± 0.006
-23.75	-23.50	0.129 ± 0.014	0.180 ± 0.011	0.215 ± 0.010	0.254 ± 0.009	0.197 ± 0.007
-23.50	-23.25	0.218 ± 0.018	0.302 ± 0.014	0.324 ± 0.012	0.354 ± 0.011	0.278 ± 0.009
-23.25	-23.00	0.359 ± 0.023	0.405 ± 0.017	0.466 ± 0.014	0.484 ± 0.013	0.382 ± 0.010
-23.00	-22.75	0.481 ± 0.027	0.570 ± 0.020	0.612 ± 0.016	0.599 ± 0.014	0.468 ± 0.012
-22.75	-22.50	0.604 ± 0.030	0.710 ± 0.022	0.757 ± 0.018	0.767 ± 0.016	0.628 ± 0.014
-22.50	-22.25	0.898 ± 0.037	0.789 ± 0.023	0.921 ± 0.020	0.906 ± 0.018	0.701 ± 0.014
-22.25	-22.00	1.098 ± 0.040	0.990 ± 0.026	1.048 ± 0.022	1.040 ± 0.019	0.760 ± 0.015
-22.00	-21.75	1.390 ± 0.046	1.114 ± 0.028	1.175 ± 0.023	1.185 ± 0.020	...
-21.75	-21.50	1.585 ± 0.049	1.264 ± 0.029	1.365 ± 0.025	1.343 ± 0.022	...
-21.50	-21.25	1.860 ± 0.053	1.393 ± 0.031	1.478 ± 0.026	1.447 ± 0.023	...
-21.25	-21.00	2.109 ± 0.056	1.469 ± 0.032	1.672 ± 0.028
-21.00	-20.75	2.383 ± 0.060	1.592 ± 0.033	1.695 ± 0.028
-20.75	-20.50	2.675 ± 0.063	1.623 ± 0.034	1.734 ± 0.028
-20.50	-20.25	3.134 ± 0.068	1.659 ± 0.034	1.825 ± 0.029
-20.25	-20.00	3.632 ± 0.074	1.672 ± 0.034
-20.00	-19.75	4.143 ± 0.079	1.677 ± 0.035
-19.75	-19.50	4.698 ± 0.084	1.717 ± 0.035
-19.50	-19.25	5.268 ± 0.090
-19.25	-19.00	5.759 ± 0.094
-19.00	-18.75	6.009 ± 0.097
-18.75	-18.50	6.531 ± 0.101
-18.50	-18.25	6.268 ± 0.100
-18.25	-18.00	5.133 ± 0.090

In order to make evolution of our SMFs more apparent, we show our maximum likelihood Schechter fits (continuous lines) and binned space densities (data points) in Figures 23 to 25 with all redshift bins on a single plot.

Table 6 shows that from $z \sim 1.1$ to $z \sim 0.3$, the characteristic space density ϕ_M^* approximately doubled for red galaxies and increased by somewhat more ($\sim \times 2.4$) for blue galaxies. At the same time, the characteristic mass M^* of both red and blue galaxies changed by no more than 0.07 dex or $\times 1.17$.

10.2. Evolution of SMD

We quantified the growth of stellar mass within the red and blue galaxy populations with the SMD, which has a clear physical meaning and is effectively the area under the SMF curve. Figure 26 and Table 6 show our results based on K -band M/L ratios. SMD is not as prone to degeneracies as the Schechter parameters. For example, we showed in Beare et al. (2015) how varying the adopted fixed value for α significantly affected the measured values of M^* and ϕ^* in the case of the B -band LF, but hardly affected the measured luminosity density at all. Similar behavior is to be expected in the equivalent case of SMFs and SMD.

We found an increase of ~ 0.37 (~ 0.31) dex in SMD for red (blue) galaxies from $z = 1.1$ to $z = 0.3$ (i.e., a factor of ~ 2.3 [~ 2.1]). We note that the red galaxy SMD growth of $\times 2.1$ implied by comparison of K -band luminosity evolution with a passively evolving stellar population (Section 9.2) is very close

to the $\times 2.3$ growth deduced here from evolution of the SMF. Figure 26 shows that for red, blue, and all galaxies, the rate at which SMD is growing decreases slowly with time. For red galaxies, this indicates that the rate at which blue galaxies move to the red sequence as they cease star formation decreases slowly with time.

10.3. Evolution of Massive Galaxies

In order to look quantitatively at the mass growth of the most massive galaxies, in Figure 27 we show the redshift evolution of stellar mass at a fixed comoving space density of $\tilde{\phi} = 2.5 \times 10^{-4} h_{70}^3 \text{ Mpc}^{-3} \text{ dex}^{-1}$. This figure is directly comparable to the evolving luminosity at fixed density shown in Figure 18. These results indicate that these most massive red galaxies grew in stellar mass from $z = 1.1$ to $z = 0.3$ by 0.23 dex (i.e., a factor of ~ 1.7). Our results also indicate stellar mass growth of 0.15 dex ($\times 1.4$) for massive blue galaxies and 0.21 dex ($\times 1.6$) for all massive galaxies, but it must be remembered that only for red galaxies is the measured stellar mass growth that for individual massive galaxies.

At a fixed space density threshold of density of $\tilde{\phi} = 2.5 \times 10^{-4} h_{70}^3 \text{ Mpc}^{-3} \text{ dex}^{-1}$, the most massive blue galaxies are ~ 0.3 dex lower in stellar mass than the most massive red galaxies (i.e., half the mass). While we expect the most massive red galaxies to remain on the red sequence and increase in mass via mergers, it is likely that the most massive

Table 10
Binned SMF for All Galaxies

log M		SMF ($h_0^3 \text{Mpc}^{-3} \log_{10} M^{-1}$)				
Min	Max	$0.2 \leq z < 0.4$	$0.4 \leq z < 0.6$	$0.6 \leq z < 0.8$	$0.8 \leq z < 1.0$	$1.0 \leq z < 1.2$
8.80	8.90	14.734 ± 0.235
8.90	9.00	14.424 ± 0.232
9.00	9.10	13.725 ± 0.226
9.10	9.20	12.765 ± 0.218
9.20	9.30	11.559 ± 0.208
9.30	9.40	11.077 ± 0.203
9.40	9.50	9.709 ± 0.190	4.011 ± 0.083
9.50	9.60	8.966 ± 0.183	3.981 ± 0.082
9.60	9.70	8.491 ± 0.178	4.134 ± 0.084
9.70	9.80	7.856 ± 0.171	4.212 ± 0.085
9.80	9.90	7.016 ± 0.162	4.102 ± 0.084
9.90	10.00	6.698 ± 0.158	4.083 ± 0.083	3.919 ± 0.065
10.00	10.10	6.489 ± 0.156	4.187 ± 0.084	3.725 ± 0.064
10.10	10.20	5.906 ± 0.149	4.187 ± 0.084	3.849 ± 0.065
10.20	10.30	5.264 ± 0.140	4.107 ± 0.084	3.761 ± 0.064
10.30	10.40	5.391 ± 0.142	4.057 ± 0.083	3.812 ± 0.064
10.40	10.50	4.946 ± 0.136	3.954 ± 0.082	3.738 ± 0.064
10.50	10.60	4.214 ± 0.125	3.802 ± 0.080	3.512 ± 0.062	2.968 ± 0.050	...
10.60	10.70	3.982 ± 0.122	3.583 ± 0.078	3.324 ± 0.060	2.633 ± 0.047	...
10.70	10.80	3.250 ± 0.110	3.321 ± 0.075	2.878 ± 0.056	2.276 ± 0.043	...
10.80	10.90	2.817 ± 0.103	2.708 ± 0.068	2.524 ± 0.052	1.827 ± 0.039	1.360 ± 0.031
10.90	11.00	2.223 ± 0.091	2.120 ± 0.060	2.022 ± 0.047	1.404 ± 0.034	1.029 ± 0.027
11.00	11.10	1.558 ± 0.076	1.443 ± 0.050	1.473 ± 0.040	0.939 ± 0.028	0.690 ± 0.022
11.10	11.20	0.997 ± 0.061	1.007 ± 0.041	0.945 ± 0.032	0.584 ± 0.022	0.402 ± 0.017
11.20	11.30	0.650 ± 0.049	0.531 ± 0.030	0.530 ± 0.024	0.315 ± 0.016	0.203 ± 0.012
11.30	11.40	0.280 ± 0.032	0.255 ± 0.021	0.276 ± 0.017	0.164 ± 0.012	0.103 ± 0.008
11.40	11.50	0.202 ± 0.027	0.133 ± 0.015	0.105 ± 0.011	0.052 ± 0.007	0.037 ± 0.005
11.50	11.60	0.075 ± 0.017	0.037 ± 0.008	0.044 ± 0.007	0.014 ± 0.003	0.013 ± 0.003
11.60	11.70	0.011 ± 0.006	0.015 ± 0.005	0.009 ± 0.003	0.006 ± 0.002	0.004 ± 0.002
11.70	11.80	...	0.005 ± 0.003	0.004 ± 0.002
11.80	11.90	0.004 ± 0.004	...	0.002 ± 0.002
11.90	12.00	0.004 ± 0.004

blue galaxies have star formation quenched and then move onto the red sequence.

The rate at which massive red galaxies increase in stellar mass through mergers with smaller galaxies appears to slow somewhat from ~ 0.4 dex per unit redshift for $z = 1.1$ to $z = 0.7$ to ~ 0.2 dex per unit redshift for $z = 0.7$ to $z = 0.3$.

We know that massive early-type galaxies must have grown in stellar mass because observations clearly show them experiencing mergers sufficient in frequency and mass ratio to give rise to a significant increase in stellar mass. In fact, merger studies have produced a range of estimates of stellar mass growth. For example, van Dokkum (2005) found a stellar mass increase due to mergers in massive red galaxies of $\Delta M/M = 0.09 \pm 0.04$ per Gyr, which implies a stellar mass increase over the 4.7 Gyr from $z = 1.1$ to $z = 0.3$ of $\times \sim 1.4$. Similarly, López-Sanjuan et al. (2012) found stellar mass growth in massive early-type galaxies due to mergers of $\times \sim 1.3$ from $z = 1$ to the present. On the other hand, Masjedi et al. (2008) found that luminous red galaxies were growing due to merger activity at a much slower rate: at least $1.7 \pm 0.1h\%$ per Gyr on average at redshift ~ 0.25 , implying at least 8% growth from $z = 1.3$ to $z = 0.3$.

The lack of evolution (in comoving coordinates) of the spatial correlation function of massive red galaxies also clearly indicates that the most massive red galaxies must be undergoing mergers. White et al. (2007) used observations of the

clustering of luminous red galaxies to show that about one-third of the most luminous satellite galaxies appear to have undergone merging or disruption with massive halos between $z = 0.9$ and $z = 0.5$, while Brown et al. (2008) found that massive red galaxies grew by $\times 1.3$ from $z = 1.0$ to $z = 0$.

As with SMD evolution, our stellar mass growth measurements for massive red galaxies based on SMF evolution ($\times 1.7$) are comparable with the those implied by comparison of the K -band LF with passive evolution ($\times 1.4$).

10.4. Stellar Mass Evolution—Errors

In addition to the sources of error inherent in measuring K -band luminosity evolution (Section 9.4), we have one very significant additional source of error in measuring stellar mass evolution—namely, uncertainty in stellar mass-to-light ratios M/L_K —and we include this in Table 5 for red galaxies. M/L_K uncertainties arise from the evolving M/L_K –rest-frame ($B-V$) relationships in Equations (3) and (5).

We take the intrinsic random variation in $\log_{10} M_K/L$ between galaxies to be 0.1 dex (Section 5). Systematic uncertainties arise from the fact that Equations (3) and (5) are derived from SPS models, and differences occur between different SPS models and the parameters used in them—notably, SFH, metallicity, and dust obscuration. A number of authors have investigated the relative impact of these different factors and arrived at various conclusions. Conroy & Wechsler (2009)

Table 11
Binned SMF for Red Galaxies

log M		SMF ($h^3 \text{Mpc}^{-3} \log_{10} M^{-1}$)				
Min	Max	$0.2 \leq z < 0.4$	$0.4 \leq z < 0.6$	$0.6 \leq z < 0.8$	$0.8 \leq z < 1.0$	$1.0 \leq z < 1.2$
8.90	9.00	1.547 ± 0.076
9.00	9.10	1.621 ± 0.078
9.10	9.20	1.887 ± 0.084
9.20	9.30	1.887 ± 0.084
9.30	9.40	2.055 ± 0.088
9.40	9.50	2.047 ± 0.087
9.50	9.60	2.081 ± 0.088	0.463 ± 0.028
9.60	9.70	2.428 ± 0.095	0.718 ± 0.035
9.70	9.80	2.413 ± 0.095	0.883 ± 0.039
9.80	9.90	2.279 ± 0.092	1.087 ± 0.043
9.90	10.00	2.544 ± 0.097	1.225 ± 0.046
10.00	10.10	2.604 ± 0.099	1.553 ± 0.051
10.10	10.20	2.548 ± 0.098	1.832 ± 0.056	1.414 ± 0.039
10.20	10.30	2.581 ± 0.098	1.887 ± 0.057	1.629 ± 0.042
10.30	10.40	2.944 ± 0.105	2.099 ± 0.060	1.916 ± 0.046
10.40	10.50	2.828 ± 0.103	2.303 ± 0.063	2.015 ± 0.047
10.50	10.60	2.720 ± 0.101	2.297 ± 0.063	2.098 ± 0.048
10.60	10.70	2.794 ± 0.102	2.343 ± 0.063	2.169 ± 0.049	1.681 ± 0.037	...
10.70	10.80	2.339 ± 0.093	2.280 ± 0.062	1.953 ± 0.046	1.545 ± 0.036	...
10.80	10.90	2.185 ± 0.090	1.875 ± 0.056	1.801 ± 0.044	1.347 ± 0.033	...
10.90	11.00	1.834 ± 0.083	1.580 ± 0.052	1.496 ± 0.040	1.068 ± 0.030	0.814 ± 0.024
11.00	11.10	1.367 ± 0.071	1.116 ± 0.044	1.126 ± 0.035	0.758 ± 0.025	0.570 ± 0.020
11.10	11.20	0.893 ± 0.058	0.845 ± 0.038	0.761 ± 0.029	0.490 ± 0.020	0.344 ± 0.015
11.20	11.30	0.598 ± 0.047	0.470 ± 0.028	0.433 ± 0.022	0.282 ± 0.015	0.184 ± 0.011
11.30	11.40	0.262 ± 0.031	0.235 ± 0.020	0.248 ± 0.016	0.147 ± 0.011	0.088 ± 0.008
11.40	11.50	0.194 ± 0.027	0.116 ± 0.014	0.086 ± 0.010	0.048 ± 0.006	0.035 ± 0.005
11.50	11.60	0.075 ± 0.017	0.034 ± 0.008	0.038 ± 0.006	0.014 ± 0.003	0.012 ± 0.003
11.60	11.70	0.011 ± 0.006	0.015 ± 0.005	0.008 ± 0.003	0.005 ± 0.002	0.003 ± 0.002
11.70	11.80	...	0.003 ± 0.002	0.002 ± 0.002
11.80	11.90	0.004 ± 0.004	...	0.001 ± 0.001
11.90	12.00	0.004 ± 0.004

found differences in stellar mass estimates of up to 0.3 dex between different models and different parameter inputs. In contrast, Moustakas et al. (2013) found that varying the SPS model, the SFH, and the metallicity had little effect, except that the inclusion of bursts of star formation in the SFH did have a significant impact on the derived SMF. Muzzin et al. (2013), surveying redshifts up to $z = 4$, found that the precise SPS model used was significant, with Maraston (2005) models producing stellar masses that are 0.2 dex lower ($\times 0.65$) than those of Bruzual & Charlot (2003) models. They also found that metallicity and delayed bursts of star formation in the SFH made little difference.

Differences in stellar mass estimates at the 0.3 dex level arising from the use of different SPS models and different SFH, metallicity, and dust model inputs constitute a very significant source of uncertainty in our measurements of stellar mass for individual galaxies. However, unless the stellar mass differences between models vary with redshift, they will not impact measurements of stellar mass evolution. We do not attempt to estimate how stellar mass differences between models might vary with redshift (if indeed they do) and therefore do not include them in total error budget for red galaxy stellar mass evolution in Table 5. Also implicit in the use of SPS models is the adoption of a specific stellar IMF (e.g., Salpeter 1955; Kennicutt 1983; Chabrier 2003). However, different choices of IMF effectively only produce offsets in calculated values of $\log_{10} M_K/L$ (i.e., stellar masses differ by constant multiplying factors). The choice of IMF does not therefore impact

conclusions regarding the percentage stellar mass growth in galaxies (Bell & de Jong 2001; Bell et al. 2003), and we do not take them into account in the total error budget for red galaxy stellar mass evolution in Table 5.

We note that although the relationship between $\log_{10} M_K/L$ and rest-frame ($B-V$) color is redshift dependent (Equations (3) and (5)), the effect of z_{phot} errors on M/L_K is small (random error of < 0.02 dex and systematic error of < 0.01 dex).

It is important to realize that the estimated errors arising from z_{phot} errors are for individual galaxies. In the case of systematic redshift errors, the impact on evolutionary measurements depends on the distribution of z_{phot} errors with redshift. Figure 1 shows that photometric redshifts are very slightly overestimated at $z \sim 0.25$ and $z \sim 0.7$, and underestimated at $z \sim 1.0$. We do not pursue this further here, beyond noting that the effect of systematic z_{phot} errors on evolutionary measurements will potentially be comparable with that on individual values.

As with our measurements of K -band luminosity evolution, in order to gauge the overall potential impact of systematic photometric redshift errors, we repeated all our calculations twice using z_{phot} values increased and decreased by the fractional systematic error over most of the redshift range (i.e., $0.2 < z \leq 1.0$), as shown in Figure 1. This was $\lambda = [z_{\text{phot}} - z_{\text{spec}}]/[1 + z_{\text{phot}}] = 0.01$. The last section of Table 5 shows that for the increased (decreased) z_{phot} values, red galaxy SMD values decreased (increased) by up to

Table 12
Binned SMF for Blue Galaxies

log M		SMF ($h_0^3 \text{Mpc}^{-3} \log_{10} M^{-1}$)				
Min	Max	$0.2 \leq z < 0.4$	$0.4 \leq z < 0.6$	$0.6 \leq z < 0.8$	$0.8 \leq z < 1.0$	$1.0 \leq z < 1.2$
8.80	8.90	13.438 ± 0.224
8.90	9.00	12.877 ± 0.219
9.00	9.10	12.104 ± 0.213
9.10	9.20	10.879 ± 0.202
9.20	9.30	9.672 ± 0.190	3.460 ± 0.077
9.30	9.40	9.022 ± 0.184	3.675 ± 0.079
9.40	9.50	7.662 ± 0.169	3.666 ± 0.079
9.50	9.60	6.885 ± 0.160	3.518 ± 0.077
9.60	9.70	6.063 ± 0.151	3.416 ± 0.076
9.70	9.80	5.443 ± 0.143	3.329 ± 0.075	3.299 ± 0.060
9.80	9.90	4.737 ± 0.133	3.015 ± 0.072	3.057 ± 0.058
9.90	10.00	4.154 ± 0.125	2.858 ± 0.070	2.860 ± 0.056
10.00	10.10	3.885 ± 0.120	2.633 ± 0.067	2.567 ± 0.053
10.10	10.20	3.358 ± 0.112	2.354 ± 0.063	2.434 ± 0.052
10.20	10.30	2.682 ± 0.100	2.220 ± 0.061	2.132 ± 0.048	1.956 ± 0.040	...
10.30	10.40	2.447 ± 0.096	1.958 ± 0.058	1.896 ± 0.045	1.726 ± 0.038	...
10.40	10.50	2.118 ± 0.089	1.650 ± 0.053	1.723 ± 0.043	1.394 ± 0.034	...
10.50	10.60	1.494 ± 0.075	1.506 ± 0.051	1.414 ± 0.039	1.206 ± 0.032	...
10.60	10.70	1.188 ± 0.067	1.240 ± 0.046	1.154 ± 0.035	0.952 ± 0.028	0.602 ± 0.020
10.70	10.80	0.912 ± 0.058	1.041 ± 0.042	0.925 ± 0.032	0.732 ± 0.025	0.489 ± 0.018
10.80	10.90	0.631 ± 0.049	0.834 ± 0.038	0.722 ± 0.028	0.480 ± 0.020	0.333 ± 0.015
10.90	11.00	0.389 ± 0.038	0.539 ± 0.030	0.526 ± 0.024	0.336 ± 0.017	0.214 ± 0.012
11.00	11.10	0.191 ± 0.027	0.327 ± 0.024	0.347 ± 0.019	0.181 ± 0.012	0.120 ± 0.009
11.10	11.20	0.105 ± 0.020	0.162 ± 0.017	0.184 ± 0.014	0.094 ± 0.009	0.057 ± 0.006
11.20	11.30	0.052 ± 0.014	0.061 ± 0.010	0.097 ± 0.010	0.033 ± 0.005	0.019 ± 0.004
11.30	11.40	0.019 ± 0.008	0.020 ± 0.006	0.028 ± 0.006	0.017 ± 0.004	0.015 ± 0.003
11.40	11.50	0.007 ± 0.005	0.017 ± 0.005	0.019 ± 0.004	0.004 ± 0.002	0.002 ± 0.001
11.50	11.60	...	0.003 ± 0.002	0.005 ± 0.002	...	0.001 ± 0.001
11.60	11.70	0.001 ± 0.001	0.001 ± 0.001	0.001 ± 0.001
11.70	11.80	...	0.002 ± 0.002	0.002 ± 0.002
11.80	11.90	0.001 ± 0.001

~ 0.03 dex, while massive red galaxies showed a stellar mass decrease (increase) of up to ~ 0.01 dex.

Again, as with K -band luminosities, to measure the effect on stellar masses of random z_{phot} errors of $\lambda = [z_{\text{phot}} - z_{\text{spec}}]/[1 + z_{\text{phot}}] = 0.05$, we repeated our calculations 10 times, each time applying normally distributed random fractional errors ($\sigma = 0.05$) to individual z_{phot} values. We found that individual measured values of both red galaxy SMD and the stellar mass of massive red galaxies differed between simulations by less than 0.01 dex, indicating that random photometric redshift errors did not produce significant scatter in these two measurements.

As with the LF, random photometric errors shift the massive end of the SMF due to Eddington bias and scattering of galaxies across redshift bin boundaries. As the penultimate section of Table 5 indicates, this shift was found to increase from ~ 0.001 at $0.2 < z \leq 0.4$ to 0.04 dex at $1.0 < z \leq 1.2$. The increase with redshift is due to the fact that the proportion of massive red galaxies with accurate spectroscopic redshifts decreases from $z \sim 0.2$ to $z \sim 1.2$.

We assume that the difference between stellar masses derived from SED fitting and those derived from the M_K/L -color relation (Equation (5)) has a scatter $\sigma = 0.1$ dex. We can measure the effect of this scatter on our results by convolving a $\sigma = 0.1$ dex Gaussian with our measured Schechter functions. We find an additional contribution of ~ 0.09 dex to the Eddington shift in the stellar mass of massive red galaxies in all redshift bins.

Monte Carlo simulations also show that random z_{phot} errors give rise to a systematic decrease in measured SMD. This systematic error ranges from ~ 0.01 dex at $0.2 < z \leq 0.4$, where a significant proportion of galaxies have accurate spectroscopic redshifts, to 0.09 dex at $1.0 < z \leq 1.2$, where few galaxies have spectroscopic redshifts. As with luminosity density (Section 9.4), the observed systematic change in SMD in each redshift bin is the net result of galaxies being scattered in and out of the bin at the upper and lower bin boundaries with perturbed stellar mass values.

Conclusion. Table 5 shows systematic errors in red galaxy SMD range from ~ 0.10 dex at $z = 0.3$ to ~ 0.18 dex at $z = 1.1$ and dominate random uncertainties of ~ 0.04 dex. Potentially, correcting for the change in systematic error with redshift could decrease the measured SMD growth from $z = 1.1$ to $z = 0.3$ by ~ 0.08 dex, altering the SMD growth from 0.37 ± 0.04 dex ($\times 2.34 \pm 0.22$) to 0.29 ± 0.04 dex ($\times 1.95 \pm 0.18$).

Systematic errors in the measured stellar mass of massive red galaxies range from ~ 0.11 dex at $z = 0.3$ to ~ 0.15 dex at $z = 1.1$ and dominate over the random errors that Monte Carlo simulations show to be less than 0.01 dex. Potentially, correcting for the change in systematic error with redshift could increase the measured stellar mass growth of massive red galaxies from $z = 1.1$ to $z = 0.3$ by ~ 0.04 dex, altering the measured growth from 0.23 ± 0.01 dex ($\times 1.70 \pm 0.04$) to 0.27 ± 0.01 dex ($\times 1.86 \pm 0.04$).

To summarize, systematic errors could have only a small effect on our conclusions for red galaxies, slightly reducing the

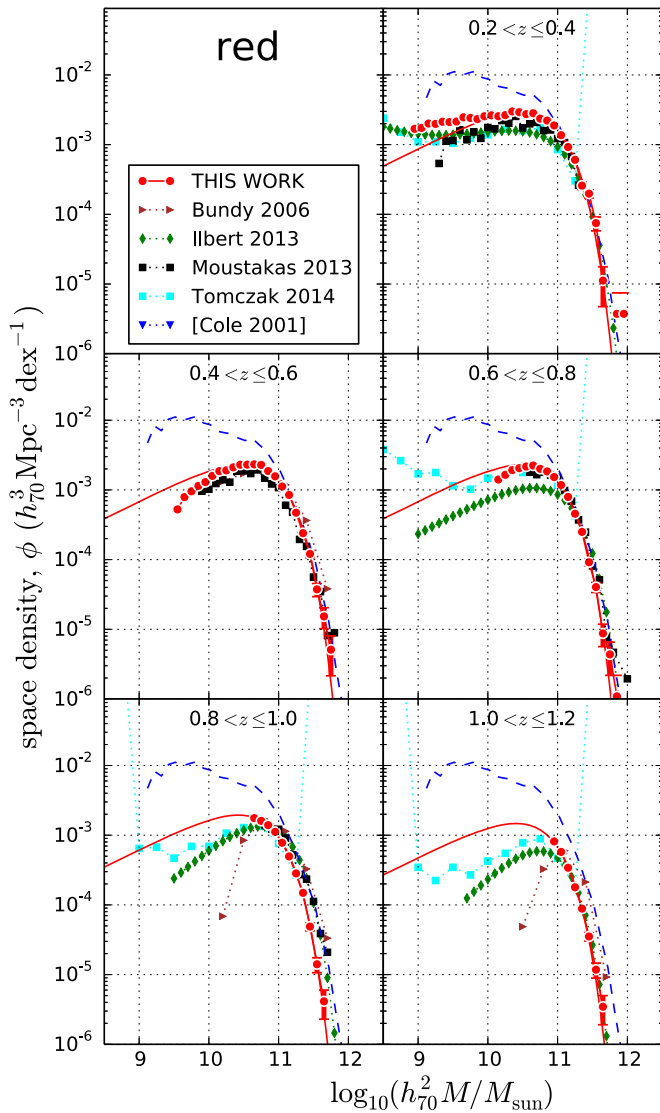


Figure 20. Binned SMFs for red galaxies based on K -band M/L ratios with $1 - \sigma$ Poisson uncertainties shown for the Boötes data. Overplotted in red are maximum likelihood fits to the (unbinned) data. We show the evolving SMFs from Bundy et al. (2006), Ilbert et al. (2013), Moustakas et al. (2013), and Tomczak et al. (2014) for comparison. The Cole et al. (2001) SMF for all galaxies in the low redshift universe is shown in the lower four plots as a black dashed line in order to provide a fixed reference. The stellar masses of the most massive red galaxies increase with time due to minor mergers.

$\times 2.3$ growth in red galaxy SMD, and slightly increasing the 70% mass growth in massive red galaxies.

10.5. Stellar Mass Evolution—Comparison with the Literature

Figures 19 and 22 show that over the mass range $9 < \log M < 11$, our SMF for all galaxies at $0.2 \leq z < 0.4$ differs by less than ~ 0.2 dex ($\sim 50\%$) in space density from other evolutionary SMF studies and from the $z < 0.2$ universe studies of Cole et al. (2001), Bell et al. (2003), and Baldry et al. (2012). As can be seen from Figure 19, the agreement with other studies is also very good at $z > 0.4$, apart from the much lower space densities seen in the $0.3 \leq z < 1.5$ VIPERS study of Davidzon et al. (2013). It is noticeable that our SMFs vary more smoothly with stellar mass than most other studies, due to our very large sample size and area.

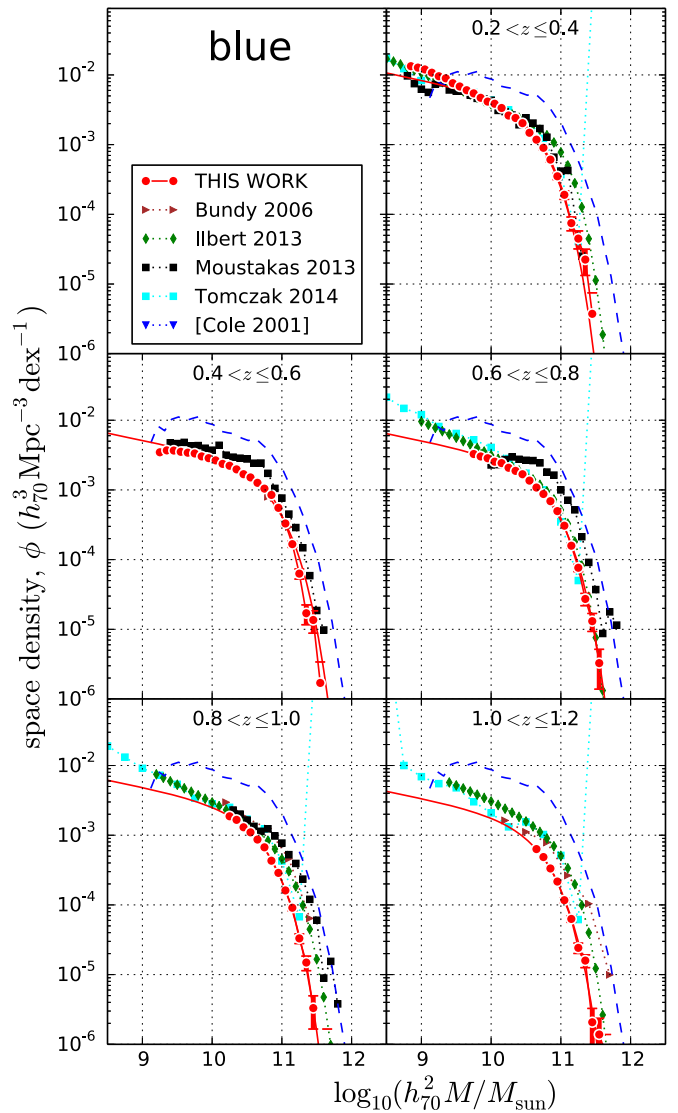


Figure 21. Binned SMFs for blue galaxies based on K -band M/L ratios with $1 - \sigma$ Poisson uncertainties shown for the Boötes data. Overplotted in red are maximum likelihood fits to the (unbinned) data. We show the evolving SMFs from Bundy et al. (2006), Ilbert et al. (2013), Moustakas et al. (2013), and Tomczak et al. (2014) for comparison. The Cole et al. (2001) SMF for all galaxies in the low redshift universe is shown in the lower four plots as a black dashed line in order to provide a fixed reference.

Figures 20 and 21 show offsets of up to 0.3 dex with the quiescent and star-forming subsamples in other studies, which may well be due to the different subsample criteria they use. We used a rest-frame color criterion, as did Bell et al. (2003), Bundy et al. (2006), Davidzon et al. (2013), and Tomczak et al. (2014), and this caused our red subsample to include dust reddened star-forming galaxies. Such galaxies were explicitly rejected by the multi-wavelength color criterion of Ilbert et al. (2013) and the SED modeling approach of Moustakas et al. (2013).

We note that there is no large difference between our SMFs and the low redshift SMFs of Cole et al. (2001) and Bell et al. (2003), despite these authors' use of 2MASS K -band luminosity values, which, even with isophotal magnitude model corrections (Section 9.5), miss much of the light from fainter outer regions of galaxies (Andreon 2002). We attribute

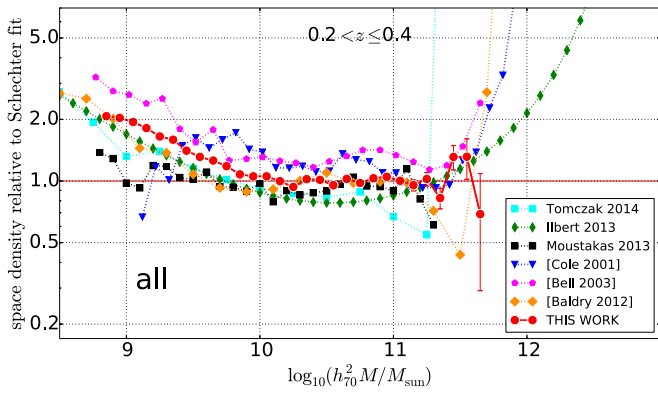


Figure 22. Detailed comparison of space densities for all galaxies at $0.2 \leq z < 0.4$ with $1 - \sigma$ Poisson uncertainties shown for the Boötes data. This displays the same data as in the top right panel of Figure 19 but plotting the ratio of binned space densities from the literature to the (unbinned) maximum likelihood Schechter function fit to our (unbinned) space densities. SMFs for the low redshift universe are labeled using square brackets. There is good agreement over most of the mass range, and we do not see a significantly greater density of very massive galaxies than other studies, even though we measure a greater density of highly luminous galaxies in the K -band (Figure 10).

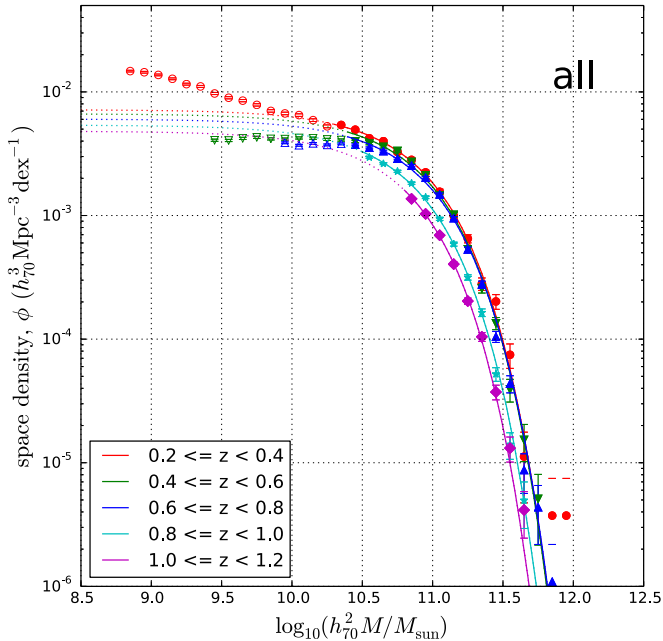


Figure 23. Evolution of the SMFs for all galaxies based on K -band M/L ratios, showing all redshift bins in one panel. Maximum likelihood fits to the (unbinned) data are shown by the continuous curves. The circles denote comoving space densities for the various mass bins. Filled circles denote the mass range used to perform the maximum likelihood fits. Open circles denote data for very low mass galaxies, which are expected to be reliable on the basis of apparent I and $[3.6 \mu\text{m}]$ magnitudes, but which are not represented adequately by a Schechter function. The error bars show $1 - \sigma$ Poisson errors for the numbers in each bin.

this agreement in measured SMFs between their work and ours to the fact that their M/L_K relationship was also calibrated using their 2MASS K -band luminosity values that are lower than those that we would measure.

In Figure 27 we compare our measurements for the mass evolution of very massive galaxies with measurements calculated using the Schechter parameters given by Bundy et al. (2006), Pérez-González et al. (2008), Muzzin et al. (2013), and Tomczak et al. (2014). For massive red galaxies,

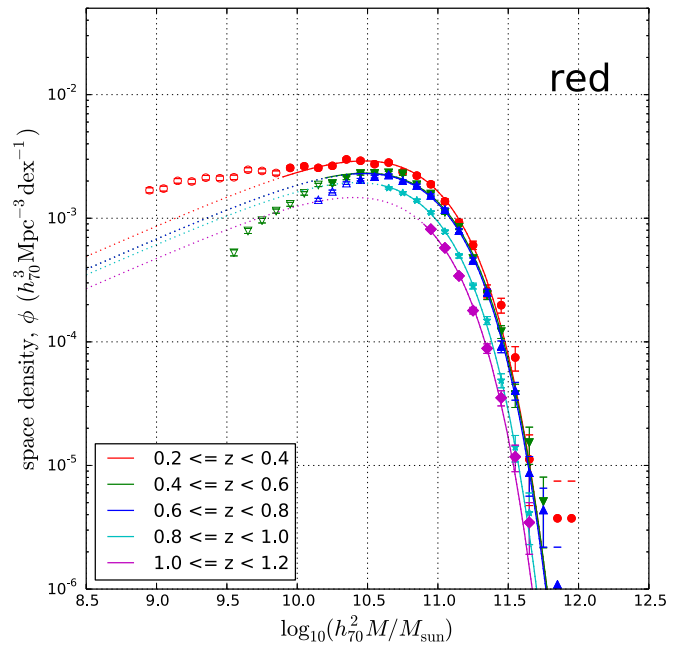


Figure 24. Evolution of the SMFs for red galaxies based on K -band M/L ratios, showing all redshift bins in one panel. Symbols are as in Figure 23. Buildup of stellar mass is evident within the red galaxy population as a whole, and growth is visible in the stellar mass of the most massive red galaxies.

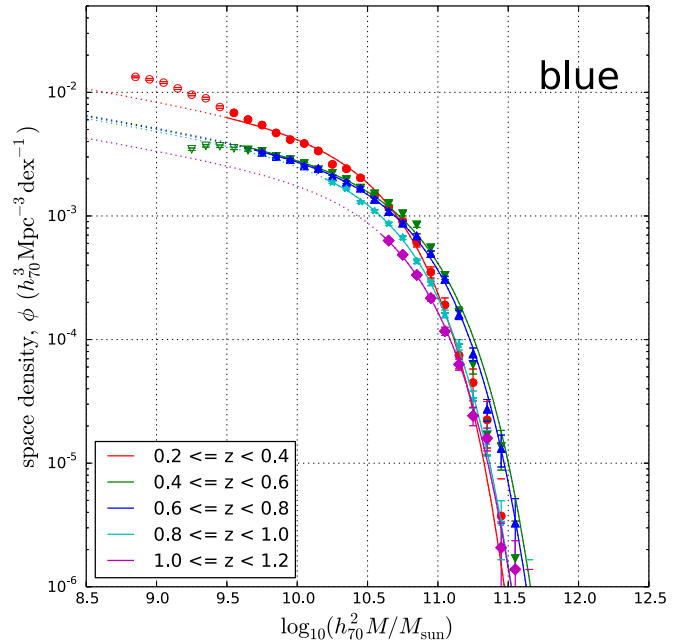


Figure 25. Evolution of the SMFs for blue galaxies based on K -band M/L ratios, showing all redshift bins in one panel. Symbols are as in Figure 23.

we see stellar mass growth of 0.23 dex ($\times 1.7$), a little more than Tomczak et al. (2014) and considerably more than Muzzin et al. (2013).

For blue galaxies, and red and blue galaxies combined, we see similar stellar mass growth (0.22 and 0.21 dex respectively), whereas many other studies see little change, except for the growth of ~ 0.16 dex seen by Muzzin et al. (2013) for red and blue galaxies combined.

Similarly, using the Stripe 82 Massive Galaxy Catalog of 41 770 massive galaxies with SDSS and UKIDSS data, Bundy et al. (2017) recently concluded that the stellar mass in all

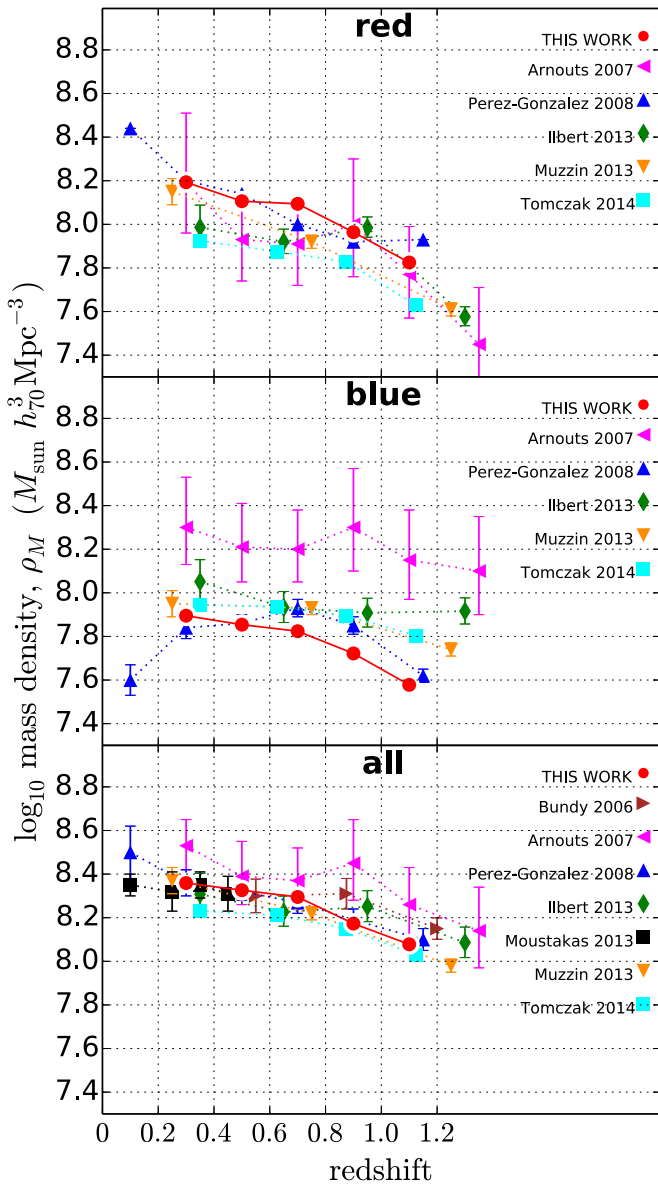


Figure 26. Evolution of the SMD based on K -band M/L ratios. From $z \sim 1.1$ to ~ 0.3 the SMD for red (blue) galaxies increases by 0.37 (0.31) dex (i.e., a factor of 2.3 [2.1]). Both red and blue galaxy SMD have grown at a steady rate. For red galaxies, this indicates that the rate at which blue galaxies move to the red sequence as they cease star formation varies little with time. For blue galaxies, it indicates that new stellar mass from star formation is almost balanced by loss of stellar mass to the red sequence as star formation ceases. Error bars on our results show errors due to cosmic variance. Error bars on results from the literature are as published.

($\log M > 11.3$) massive galaxies changed by less than 9% from $z = 0.65$ to $z = 0.3$. They investigated in detail several potential sources of random and systematic error in the determination of stellar masses from photometry, including photometric redshift errors, differences due to the use of different SPS models, and differences due to differing assumed star formation histories in SPS models. They concluded that the latter source of error was the most significant. However, they also speculated missing light in their photometry could strongly impact their conclusions.

It must be remembered that the results of other studies of massive galaxies are based on Schechter fits to the whole of the measured SMF, whereas we have based our mass growth

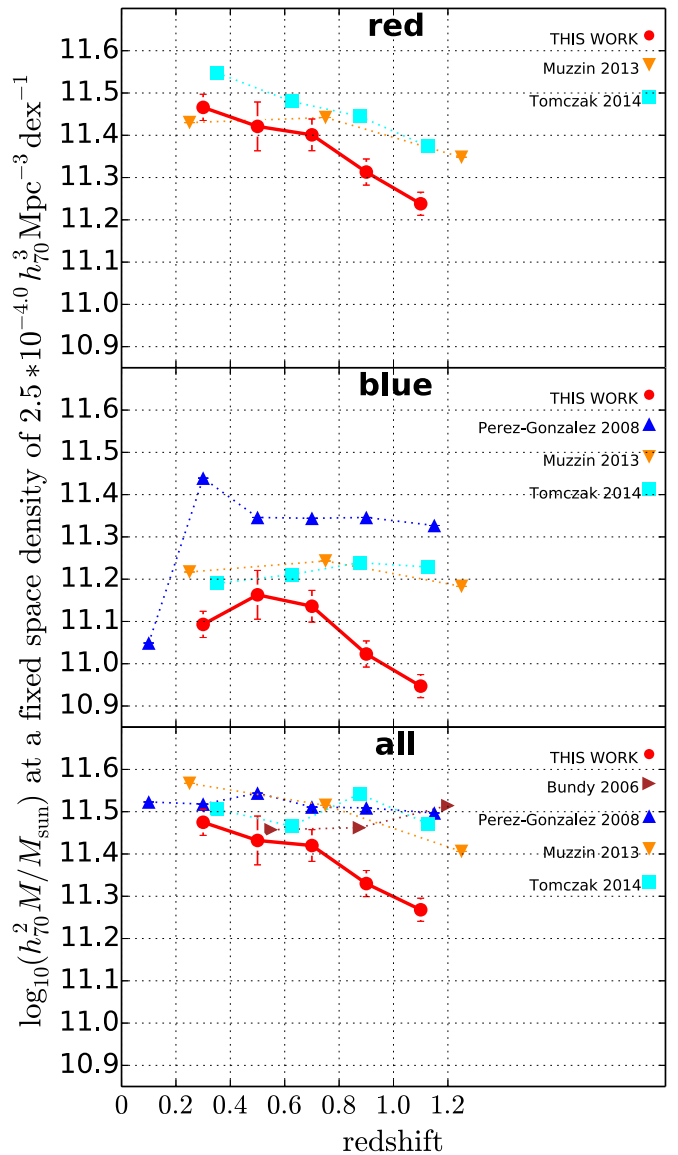


Figure 27. Evolution of very massive galaxies based on K -band M/L ratios. From $z \sim 1.1$ to ~ 0.3 the masses of the most massive red (blue) galaxies increased by 0.23 (0.16) dex (i.e., a factor of 1.7 [1.4]). The rate at which massive red galaxies increased in stellar mass through mergers with smaller galaxies appears to have slowed somewhat from ~ 0.4 dex per unit redshift for $z = 1.1$ to $z = 0.7$ to ~ 0.2 dex per unit redshift for $z = 0.7$ to $z = 0.3$. The value of $h_{70}^2 \log_{10} M/M_{\odot}$ corresponding to a fixed space density of $2.5 \times 10^{-4.0} h_{70}^3 \text{Mpc}^{-3} [\log_{10} M]^{-1}$ effectively measures the evolution of the most massive galaxies. Results from the literature have been computed using the published Schechter parameters when available. Error bars on our results show errors due to cosmic variance. Error bars on results from the literature are as published.

measurements on variable α Schechter fits to just the massive end of the SMF. This will be considerably more accurate, as we have only been using the Schechter parameterization as a tool to produce a very close fit in order to measure a small section of the SMF at the high mass end (Section 8).

11. Summary

We measured evolution of the K -band LF and the galaxy SMF from $z = 1.2$ to $z = 0.2$ using a very large sample of 353 594 galaxies covering a large area of 8.26 deg^2 in Boötes, surveyed to a depth of $I = 24$. The imaging, catalogs, and

photometry were identical to those in Beare et al. (2015) and derived from various optical and infrared surveys. Our very large sample size and area minimized both Poisson errors and the effects of cosmic variance ($\sim 3\%$ for all galaxies and $\sim 8\%$ for red galaxies, which are more strongly clustered).

We used a magnitude dependent aperture diameter and curve of growth analysis to measure precise photometry in 13 optical and infrared bands. Using this photometry and the 129 SED templates from Brown et al. (2014), we were able to precisely determine photometric redshifts (and luminosity distances) using the Bayesian EAZY code.

Galaxy luminosities were derived from apparent magnitudes and redshifts using the method of Beare et al. (2014) and the 129 SED templates of Brown et al. (2014). We used GAMA/G10 COSMOS data to derive the evolving dependence of K -band mass-to-light ratios on rest-frame ($B-V$) color and used this to measure stellar masses.

Binned K -band LFs and SMFs were produced for five redshift bins between $z = 0.2$ and $z = 1.2$ and found to be consistent with LFs and SMFs from the literature. LF and SMF evolution were measured using maximum likelihood Schechter function fits within each redshift bin. Red and blue galaxies were differentiated using an evolving rest-frame ($U - B$) color-magnitude cut, as in Beare et al. (2015).

Luminosity densities and stellar mass densities were calculated from the Schechter parameters, and their evolution was measured. Evolution of the bright end of the LF and the massive end of the SMF were measured by finding the luminosity and stellar mass, respectively, corresponding to a fixed space density. This was done by fitting a maximum likelihood Schechter function with variable α parameter to the luminous and massive ends of the LF and SMF, respectively.

As a main focus of our work has been to measure evolution of the K -band luminosity and the stellar mass of red galaxies, we made detailed estimates of the various random and systematic errors for red galaxies, tabulating these in Table 5.

The total luminosity density of both red and blue galaxies increased by a modest 0.08 dex (i.e., a factor of 1.2, from $z = 1.1$ to $z = 0.3$). Over the same redshift range, the luminosity of highly luminous red (blue) galaxies decreased by 0.19 (0.33) mag, which equates to 0.08 (0.13) dex or a factor of $\times 0.83$ ($\times 0.74$). Highly luminous red galaxies fade at an ever-increasing rate from $z \sim 1.1$ to $z \sim 0.3$. Comparison with a passively evolving population implied a factor of ~ 2.1 growth in red galaxy SMD, and a factor of ~ 1.4 growth in the stellar mass of highly luminous massive red galaxies.

Using our evolving SMFs, we found an increase of 0.37 (0.31) dex in SMD for red (blue) galaxies (i.e., a factor 2.3 [2.1]), from $z = 1.1$ to $z = 0.3$. The rate at which SMD is growing decreases slowly with time. For red galaxies, this indicates that the rate at which blue galaxies move to the red sequence as they cease star formation decreases slowly with time.

The mass of the most massive red (blue) galaxies increased by 0.23 (0.15) dex (i.e., a factor of $\times 1.7$ [$\times 1.4$]), from $z = 1.1$ to $z = 0.3$. The rate at which massive red galaxies increase in stellar mass through mergers with smaller galaxies slows from ~ 0.4 dex per unit redshift for $z = 1.1$ to $z = 0.7$ to ~ 0.2 dex per unit redshift for $z = 0.7$ to $z = 0.3$.

We thank the anonymous referee for suggestions that have greatly improved the quality of our results and enhanced the

clarity of this paper. R.B. wishes to thank Monash University for financial support from MGS and MIPRS postgraduate research scholarships. M.B. acknowledges financial support from the Australian Research Council (FT100100280) and the Monash Research Accelerator Program (MRA). K.P. acknowledges the support of STFC, through the University of Hull's Consolidated Grant ST/R000840/1. We thank colleagues on the NDWFS, SDWFS, NEWFIRM Boötes, and AGES teams, in particular M. L. N. Ashby, R. J. Cool, A. Dey, P. R. Eisenhardt, D. J. Eisenstein, A. H. Gonzalez, B. T. Jannuzi, C. S. Kochanek, and D. Stern. This work is based in part on observations made with the *Spitzer Space Telescope*, which is operated by the Jet Propulsion Laboratory, California Institute of Technology, under a contract with NASA. This research was supported by the National Optical Astronomy Observatory, which is operated by the Association of Universities for Research in Astronomy (AURA), Inc., under a cooperative agreement with the National Science Foundation.

ORCID iDs

Michael J. I. Brown  <https://orcid.org/0000-0002-1207-9137>

References

- Andreon, S. 2002, *A&A*, 382, 495
- Andrews, S. K., Driver, S. P., Davies, L. J. M., et al. 2017, *MNRAS*, 464, 1569
- Arnouts, S., Walcher, C. J., Le Fèvre, O., et al. 2007, *A&A*, 476, 137
- Ashby, M. L. N., Stern, D., Brodwin, M., et al. 2009, *ApJ*, 701, 428
- Baldry, I. K., Driver, S. P., Loveday, J., et al. 2012, *MNRAS*, 421, 621
- Beare, R., Brown, M. J. I., & Pimbblet, K. 2014, *ApJ*, 797, 104
- Beare, R., Brown, M. J. I., Pimbblet, K., Bian, F., & Lin, Y.-T. 2015, *ApJ*, 815, 94
- Bell, E. F., & de Jong, R. S. 2001, *ApJ*, 550, 212
- Bell, E. F., McIntosh, D. H., Katz, N., & Weinberg, M. D. 2003, *ApJS*, 149, 289
- Bell, E. F., Wolf, C., Meisenheimer, K., et al. 2004, *ApJ*, 608, 752
- Bennett, C. L., Larson, D., Weiland, J. L., et al. 2013, *ApJS*, 208, 20
- Bernardi, M., Meert, A., Sheth, R. K., et al. 2016, *MNRAS*, 455, 4122
- Bertin, E., & Arnouts, S. 1996, *A&AS*, 117, 393
- Bian, F., Fan, X., Jiang, L., et al. 2013, *ApJ*, 774, 28
- Blanton, M. R., & Roweis, S. 2007, *AJ*, 133, 734
- Bonne, N. J., Brown, M. J. I., Jones, H., & Pimbblet, K. A. 2015, *ApJ*, 799, 160
- Borch, A., Meisenheimer, K., Bell, E. F., et al. 2006, *A&A*, 453, 869
- Brammer, G. B., van Dokkum, P. G., & Coppi, P. 2008, *ApJ*, 686, 1503
- Brammer, G. B., Whitaker, K. E., van Dokkum, P. G., et al. 2011, *ApJ*, 739, 24
- Brown, M. J. I., Dey, A., Jannuzi, B. T., et al. 2007, *ApJ*, 654, 858
- Brown, M. J. I., Moustakas, J., Smith, J. D. T., et al. 2014, *ApJS*, 212, 18
- Brown, M. J. I., Zheng, Z., White, M., et al. 2008, *ApJ*, 682, 937
- Bruzual, G., & Charlot, S. 2003, *MNRAS*, 344, 1000
- Bundy, K., Ellis, R. S., Conselice, C. J., et al. 2006, *ApJ*, 651, 120
- Bundy, K., Leauthaud, A., Saito, S., et al. 2017, *ApJ*, 851, 34
- Calvi, V., Stiavelli, M., Bradley, L., Pizzella, A., & Kim, S. 2014, *ApJ*, 796, 102
- Calzetti, D., Armus, L., Bohlin, R. C., et al. 2000, *ApJ*, 533, 682
- Chabrier, G. 2003, *PASP*, 115, 763
- Cirasuolo, M., McLure, R. J., Dunlop, J. S., et al. 2010, *MNRAS*, 401, 1166
- Cirasuolo, M., McLure, R. J., Dunlop, J. S., et al. 2007, *MNRAS*, 380, 585
- Cole, S., Norberg, P., Baugh, C. M., et al. 2001, *MNRAS*, 326, 255
- Conroy, C., & Wechsler, R. H. 2009, *ApJ*, 696, 620
- Cowie, L. L., Songaila, A., Hu, E. M., & Cohen, J. G. 1996, *AJ*, 112, 839
- Croton, D. J. 2013, *PASA*, 30, 52
- Croton, D. J., Springel, V., White, S. D. M., et al. 2006, *MNRAS*, 365, 11
- da Cunha, E., Charlot, S., & Elbaz, D. 2008, *MNRAS*, 388, 1595
- D'Souza, R., Vegetti, S., & Kauffmann, G. 2015, *MNRAS*, 454, 4027
- Davidzon, I., Bolzonella, M., Coupon, J., et al. 2013, *A&A*, 558, A23
- Davies, L. J. M., Driver, S. P., Robotham, A. S. G., et al. 2015, *MNRAS*, 447, 1014
- Devereux, N., Willner, S. P., Ashby, M. L. N., Willmer, C. N. A., & Hriljac, P. 2009, *ApJ*, 702, 955
- Driver, S. P., Hill, D. T., Kelvin, L. S., et al. 2011, *MNRAS*, 413, 971

- Driver, S. P., Robotham, A. S. G., Kelvin, L., et al. 2012, *MNRAS*, 427, 3244
- Drory, N., Bender, R., Feulner, G., et al. 2003, *ApJ*, 595, 698
- Drory, N., Bundy, K., Leuthaud, A., et al. 2009, *ApJL*, 707, L1595
- Drory, N., Salvato, M., Gabasch, A., et al. 2005, *ApJL*, 619, L131
- Eddington, A. S. 1913, *MNRAS*, 73, 359
- Eisenhardt, P. R. M., Brodwin, M., Gonzalez, A. H., et al. 2008, *ApJ*, 684, 905
- Eke, V. R., Baugh, C. M., Cole, S., et al. 2005, *MNRAS*, 362, 1233
- Fioc, M., & Rocca-Volmerange, B. 1997, *A&A*, 326, 950
- González, V., Labbé, I., Bouwens, R. J., et al. 2011, *ApJL*, 735, L34
- Guo, Q., & White, S. D. M. 2008, *MNRAS*, 384, 2
- Hill, D. T., Driver, S. P., Cameron, E., et al. 2010, *MNRAS*, 404, 1215
- Huang, J.-S., Glazebrook, K., Cowie, L. L., & Tinney, C. 2003, *ApJ*, 584, 203
- Ilbert, O., Salvato, M., Le Floch, E., et al. 2010, *ApJ*, 709, 644
- Ilbert, O., Salvato, M., Le Floch, E., et al. 2013, *A&A*, 556, A55
- Jannuzi, B. T., & Dey, A. 1999, in ASP Conf. Ser. 191: Photometric Redshifts and the Detection of High Redshift Galaxies, ed. R. Weymann et al. (San Francisco, CA: ASP), 111
- Jarrett, T. H., Chester, T., Cutri, R., et al. 2000, *AJ*, 119, 2498
- Jones, D. H., Peterson, B. A., Colless, M., & Saunders, W. 2006, *MNRAS*, 369, 25
- Kelvin, L. S., Driver, S. P., Robotham, A. S. G., et al. 2014, *MNRAS*, 439, 1245
- Kennicutt, R. C., Jr. 1983, *ApJ*, 272, 54
- Kochanek, C. S., Eisenstein, D. J., Cool, R. J., et al. 2012, *ApJS*, 200, 8
- Kochanek, C. S., Pahre, M. A., Falco, E. E., et al. 2001, *ApJ*, 560, 566
- Lacey, C. G., Baugh, C. M., Frenk, C. S., et al. 2016, *MNRAS*, 462, 3854
- Li, C., & White, S. D. M. 2009, *MNRAS*, 398, 2177
- Liske, J., Baldry, I. K., Driver, S. P., et al. 2015, *MNRAS*, 452, 2087
- López-Sanjuan, C., Díaz-García, L. A., Cenarro, A. J., et al. 2019, *A&A*, 622, A51
- López-Sanjuan, C., Le Fèvre, O., Ilbert, O., et al. 2012, *A&A*, 548, A7
- Loveday, J. 2000, *MNRAS*, 312, 557
- Loveday, J., Norberg, P., Baldry, I. K., et al. 2015, *MNRAS*, 451, 1540
- Maraston, C. 2005, *MNRAS*, 362, 799
- Maraston, C., Pforr, J., Henriques, B. M., et al. 2013, *MNRAS*, 435, 2764
- Marshall, H. L., Tananbaum, H., Avni, Y., & Zamorani, G. 1983, *ApJ*, 269, 35
- Masjedi, M., Hogg, D. W., & Blanton, M. R. 2008, *ApJ*, 679, 260
- Miyazaki, S., Komiyama, Y., Nakaya, H., et al. 2012, *Proc. SPIE*, 8446, 84460Z
- Mortlock, A., Conselice, C. J., Bluck, A. F. L., et al. 2011, *MNRAS*, 413, 2845
- Mortlock, A., McLure, R. J., Bowler, R. A. A., et al. 2017, *MNRAS*, 465, 672
- Moustakas, J., Coil, A. L., Aird, J., et al. 2013, *ApJ*, 767, 50
- Muzzin, A., Marchesini, D., Stefanon, M., et al. 2013, *ApJ*, 777, 18
- Pérez-González, P. G., Rieke, G. H., Villar, V., et al. 2008, *ApJ*, 675, 234
- Pozzetti, L., Cimatti, A., Zamorani, G., et al. 2003, *A&A*, 402, 837
- Salpeter, E. E. 1955, *ApJ*, 121, 161
- Schaye, J., Crain, R. A., Bower, R. G., et al. 2015, *MNRAS*, 446, 521
- Schechter, P. 1976, *ApJ*, 203, 297
- Smith, A. J., Loveday, J., & Cross, N. J. G. 2009, *MNRAS*, 397, 868
- Springel, V., White, D. M., Jenkins, A., et al. 2005, *Natur*, 435, 629
- Stern, D., Eisenhardt, P., Gorjian, V., et al. 2005, *ApJ*, 631, 163
- Taylor, E. N., Franx, M., van Dokkum, P. G., et al. 2009, *ApJS*, 183, 295
- Taylor, E. N., Hopkins, A. M., Baldry, I. K., et al. 2011, *MNRAS*, 418, 1587
- Tomczak, A. R., Quadri, R. F., Tran, K. V. H., et al. 2014, *ApJ*, 783, 85
- van Dokkum, P. G. 2005, *AJ*, 130, 2647
- Vogelsberger, M., Genel, S., Springel, V., et al. 2014, *Natur*, 509, 177
- White, M., Zheng, Z., Brown, M. J. I., Dey, A., & Jannuzi, B. T. 2007, *ApJL*, 655, L69
- Wright, A. H., Robotham, A. S. G., Bourne, N., et al. 2016, *MNRAS*, 460, 765